ATTACHMENT B

REMARKS

By this amendment, in conjunction with the RCE filed herewith, Applicants have now amended Claims 17-21 by adopting the suggestions of the Examiner to overcome minor objections as discussed below. In light of the amendments and arguments provided herein, Applicants submit that the present application has been placed in condition for allowance for the reasons as set forth below.

In the Official Action, the Examiner objected to Claim 19 under 35 U.S.C. §112 on the basis of new matter, but at the same time acknowledged that there is support in the application for a method of treating or preventing pathological conditions associated with overstimulation of T-cells. Accordingly, without addressing the objections of the Examiner, the Examiner's rejection has no become moot in light of the fact that Applicants have amended the claims to the terms the Examiner has acknowledged are supported in the specification.

In the Official Action, the Examiner also made several minor rejections under 35 U.S.C. §112, second paragraph, with regard to the language of the claims. Without addressing the merits of the Examiner's objections in this regard, Applicants have overcome the rejections in all cases by adopting as needed the suggestions of the Examiner or amending the language of the claims to avoid the rejections. Applicants submit that the claims are amended are in compliance with 35 U.S.C. §112, second paragraph, and that those rejections are respectfully traversed.

Finally, in the Official Action, the Examiner rejected the claims under 35 U.S.C. §112, first paragraph, on the grounds that there was a lack of enablement. In particular,

the Examiner indicated that the specification would not be predictive of successful results in human systems and that it has not yet been shown that the Map protein of the invention can be used to treat "all encompassed T cell lymphoproliferative diseases and conditions associated with overstimulation of T cells in a human or non-human host." In short, this rejection is respectfully traversed in that the presently claimed invention has indeed been shown repeatedly in many different systems and models to be effective in suppressing T-cell proliferation and thus treating or preventing the conditions associated with T cell proliferation, and that one skilled in the art would readily be able to practice the invention without undue experimentation.

As set forth in Applicants' specification, the present invention relates to Applicants' novel and unexpected discovery that the Map protein (also known as the extracellular adherence protein or EAP) was able to act as an immunomodulator so as to be able to suppress or prevent the proliferation of T cell-mediated responses in human or animal patients. In this regard, as also shown in the specification, several different T-cell-stimulating bacterial antigens were used in tests to determine whether the introduction of the Map could be used to suppress T-cell proliferation, and in all of these cases, both in vitro and in vivo, T-cell proliferation was suppressed.

In one case, administration of Map was shown to be a successful immunomdoulatory protein in double infection studies in which a primary infection with $Map^{-}SA$ conferred significant protection against reinfection with $Map^{+}SA$. This contrasts significantly with SA-induced pathology from mice receiving primary and secondary infections with $Map^{+}SA$. Accordingly, T cell-mediated responses in $Map^{+}SA$-infected mice were suppressed in the presence of Map compared to $Map^{-}SA$ -infected mice

which develop cell-mediated immunity over the course of infection. In addition, flow cytometric analysis of fluorescein isothiocyanate (FITC)-labeled Map19 revealed that this antigen was bound to 100% of BAT2.2 T cells, once again confirming that Map will bind to T cells and suppress their proliferation following presentation of a T-cell stimulating antigen.

Even further studies were done whereby nylon wool-purified naive T cells were cultured in the presence of Map19 were not induced to either proliferate or undergo apoptosis. Accordingly, the tests described in the specification showed to one skilled in the art that Map was able to function as an immunoregulatory protein during SA infections and other introductions of antigens that stimulate T-cell proliferation and thus that it could be used to treat or prevent conditions associated with T-cell proliferation. The results were so significant that the information concerning the present invention was accepted in a prestigious journal and published in the *Journal of Clinical Investigation*, Vol. 110 (10):14651471 (2002) (Copy attached as Appendix 1). In summary, Applicants had already shown to one skilled in the art that despite the fact that different antigens were introduced which had different modes of T-cell stimulation that Map was successful in all of these contexts in suppressing T-cell stimulation, and thus one skilled in the art would have expected that introduction of an effective amount of Map would be useful in conditions associated with T-cell proliferation.

However, further independent studies including those involving a human system involving T-cell recognition and proliferation have shown that the present invention operates in conditions that would be recognized as illustrative of its capabilities to treat or prevent such T cell proliferation in humans. In particular, additional groups studying

the Map (or Eap) protein have tested its ability to suppress T-cell proliferation and associated pathological conditions affecting humans and have found that it is effective in treating or preventing those conditions in the manner set forth in Applicants' specification. Specifically, in the Xie et al. journal article, *Journal of Experimental Medicine* , Apr 17;203(4):985-94 (2006), studies were conducted using an animal model having the condition of experimental encephalomyelitis (EAE) which mimics the conditions of MS in humans. In particular, this is an autoimmune disease wherein T cells react and proliferate against myelin components, and the mouse EAE model reflects conditions wherein T cells are induced by myelin so as to attack the central nervous system. In these studies, Map was used as therapy against T-cell proliferation in the EAE models which would reflect the disease MS in human patients, and indeed the test conditions were adjusted so as to be reflective of human conditions. As shown in the attached article, under conditions equivalent to a clinical setting of MS, the article reported that

> Strikingly, intervention with [Map] after to onset of EAE . . . resulted in a prompt clinical recovery from EAE, which was significant eve 2 d after the first [Map] administration. . .In addition, consistent with our data and with the dramatic inhibitory effect on the clinical EAE symptoms by [Map], we found that mononuclear cell infiltrates were strongly reduced or almost absent in the brains of [Map]-treated mice compared with the vehicle-treated mice that presented with perivascular and parenchymal inflammatory cell infiltrates. Furthermore, the T cell recruitment to the brain was inhibited by [Map] as indicated by the significant decrease in staining for CD3 in the brains of [Map]-treated mice as compared with the brains of vehicle-treated mice (Fig. 6). Collectively, [Map] prevented the development of EAE, as well as reverted the disease after its onset as a result of the propensity of the protein to block the infiltration of inflammatory T cells into the brain.

See Appendix 2, page 5. It is well established in the field that the EAE mouse model is accepted for testing on Multiple Sclerosis (MS). See Appendix 3.

Accordingly, as set forth in Xie et al., as disclosed in Applicants' specification, the present invention was useful to treat a system that modeled the human MS disease conditions in which T cells which recognized the human protein myelin were suppressed by the addition of the Map protein so as to treat or prevent the pathological conditions associated with MS. In this regard, the Examiner's contention that one skilled in the art would be limited to use in bacterial antigenic systems is clearly refuted.

Even further, the Xie et al. article disclosed that as an initial test of the efficacy of Map in suppressing T cell proliferation, another T-cell inducing antigen, namely oxazolone, was introduced into mice who accordingly produced a DTH response and specific inflammation at the site of the challenge. In each of the tests, the introduction of Map showed that the treated mice "had a significantly reduced DTH response as compared with vehicle-treated but immunized control mice" and "significantly reduced Eva's blue leakage by 50-60%." Once again, in a further system with yet another different T-cell stimulated antigen, the results confirmed that the present invention can be used to suppress T cell stimulation whether based on bacterial antigens or mammalian antigens, and once again that one skilled in the art would have been enabled to carry out the claimed invention as disclosed in the specification. In short, in cases after case involving different antigens, including bacterial and mammalian, in different systems and tests, it has been repeatedly shown that the administration of Map in accordance with the present invention is effective in suppressing T-cell proliferation in a variety of contexts and conditions.

Moreover, with regard to whether or not there is "undue experimentation" in any particular case so as to support a rejection under the enablement provision of Section

112, the one case which is the standard by which an enablement rejection must be assessed is the Federal Circuit decision of In re Wands which established the criteria for a determination of whether a claim in objectionable on the basis of undue experimentation, and which the Examiner cited in the Official Action for this basis. Notably, In re Wands, 8 U.S.P.Q.2d 1400 (Fed. Cir. 1988) was a case wherein the original Examiner and the Patent Board of Appeals had claimed there was "undue experimentation" because some screening and experimentation was necessary to obtain the high-binding monoclonal antibodies in accordance with the claims and thus practice the invention. In the examples disclosed in the specification, out of an original 143 hybridomas prepared in accordance with the invention, only 9 were deemed suitable for further analysis, and only 4 of these were shown to have the high binding affinity needed for the antibodies of the claims. The Examiner and Board had argued that since only 4 of 143 hybridomas had been shown to operate in the claimed manner, the fact that only a few successful examples were included meant that there was undue experimentation involved for one skilled in the art to practice the invention.

However, despite the fact that multiple experiments were necessary to obtain antibodies which met the requirements of the claims, and despite the fact that the experiments led to many attempts which did not result in the claimed antibodies, the Federal Circuit **reversed** the Examiner and the Board and held that the claims were in fact enabled. The key element of the decision held that because there was reasonable guidance provided in the application, and because any necessary experimentation was simply **routine** one of ordinary skill in the art, any such experimentation was not "undue." In particular, the Federal Circuit held that the test for "undue experimentation"

was not merely quantitative, but instead was based on whether any experimentation needed was **routine**. As the Court stated, "the test is not merely quantitative, since a considerable amount of experimentation is permitted, **if it merely routine**, or if the specification provides a reasonable amount of guidance with respect to the direction in which the experimentation should proceed." 8 U.S.P.Q.2d at 1404 (emphasis added). Accordingly, the Federal Circuit held that there was **no** "undue experimentation" necessary to make and use the invention because the Applicants had provided "considerable direction and guidance on how to practice their invention and provided working examples" and because practitioners in this art were well prepared to screen hybridomas in order to find one that made the desired antibody. 8 U.S.P.Q.2d at 1406.

In the present case, Applicants provide specific guidance that is well sufficient for one skilled in the art to make and use the invention which is the utilization of an effective amount of the Map protein to suppress T-cell proliferation so as to treat or prevent the pathological conditions associated with such proliferation. Indeed, it is clear that the techniques used to carry out the invention, particularly in the present filed where the level of skill is extremely high, are well within the capability of the ordinary practitioner in the art and will require at most routine screening using methods well known in the art. Since it is well recognized that it is **routine** and well within the skill of the ordinary artisan to determine at what level the administration of the Map protein in the present invention will be necessary to reduce or eliminate T-cell proliferation in the response to a T-cell stimulus, whether bacterial or mammalian, the established criteria of the Wands case would **preclude** a rejection in the present application on the basis of undue

experimentation since where "routine" experimentation is all that is necessary, the experimentation cannot be considered "undue."

Moreover, in contrast to the Examiner's contention regarding the scope of the claims and the need to show enablement for every possible embodiment, such a position is contrary to law. Indeed, it has been held that the first paragraph of 35 U.S.C. §112 requires nothing more than objective enablement, and that this teaching may be set forth by the use of illustrative examples or broad descriptive terminology. The specification which teaches how to make and use the invention in terms that correspond to the scope of the claims *must* be taken as complying with the first paragraph of 35 USC 112 *unless* there is reason to doubt the objective truth of the statements relied upon therein for establishing enablement. Staehelin v, Secher, 24 U.S.P.Q.2d 1513 (Bd. Pat. App. Int. 1992) (emphasis in original); See also In re Marzocchi, 169 USPQ 367 (CCPA 1971). In the present case, not only is there no reason to doubt the objective truth of the specification with regard to the applications of the present claims, indeed further evidence upon a mouse model that simulates the human MS condition has confirmed Applicants' description regarding the use of the present invention to treat or prevent pathological conditions associated with T-cell proliferation.

Accordingly, it is clear that the present specification will enable one skilled in the art to make and use the present claimed invention without undue experimentation, see Hybritech Inc. v. Monoclonal Antibodies, Inc., 231 USPQ 81 (Fed. Cir. 1986), and has already been practiced in the field by skilled artisans using standard techniques as reflected above. Applicants thus submit that the Examiner's rejection under 35 U.S.C. §112 on the basis of "undue experimentation" is improper and should be withdrawn.

In light of the amendments and arguments as set forth above, Applicants submit that the present application overcomes all prior rejections and has been placed in condition for allowance. Such action is earnestly solicited.

END OF REMARKS

APPENDIX 1

The *Staphylococcus aureus* Map protein is an immunomodulator that interferes with T cell–mediated responses

Lawrence Y. Lee,[1] Yuko J. Miyamoto,[2] Bradley W. McIntyre,[2] Magnus Höök,[1] Kirk W. McCrea,[1] Damien McDevitt,[1] and Eric L. Brown[1]

[1]The Center for Extracellular Matrix Biology, Texas A&M University System Health Science Center, Albert B. Alkek Institute of Biosciences and Technology, Houston, Texas, USA
[2]Department of Immunology, The University of Texas M.D. Anderson Cancer Center, Houston, Texas, USA

Staphylococcus aureus (SA) is an opportunistic pathogen that affects a variety of organ systems and is responsible for many diseases worldwide. SA express an MHC class II analog protein (Map), which may potentiate SA survival by modulating host immunity. We tested this hypothesis in mice by generating Map-deficient SA (Map$^-$SA) and comparing disease outcome to wild-type Map$^+$SA–infected mice. Map$^-$SA–infected mice presented with significantly reduced levels of arthritis, osteomyelitis, and abscess formation compared with control animals. Furthermore, Map$^-$SA–infected nude mice developed arthritis and osteomyelitis to a severity similar to Map$^+$SA–infected controls, suggesting that T cells can affect disease outcome following SA infection and Map may attenuate cellular immunity against SA. The capacity of Map to alter T cell function was tested more specifically in vitro and in vivo using native and recombinant forms of Map. T cells or mice treated with recombinant Map had reduced T cell proliferative responses and a significantly reduced delayed-type hypersensitivity response to challenge antigen, respectively. These data suggest a role for Map as an immunomodulatory protein that may play a role in persistent SA infections by affecting protective cellular immunity.

J. Clin. Invest. **110**:1461–1471 (2002). doi:10.1172/JCI200216318.

Introduction

Staphylococcus aureus (SA) is an opportunistic pathogen that colonizes the skin (primarily the anterior nasal vestibule) of approximately 20% of the population without causing clinical symptoms (1, 2). If, however, the skin is damaged by trauma, inoculation by needles, or direct implantation of medical devices, SA can gain entry into the host and colonize and infect a variety of tissues (3). SA can cause lethal infections often associated with abscess formation such as endocarditis and pneumonia. Due to a developing resistance to multiple antibiotics, SA is recognized worldwide as a major health threat (2, 4–7).

Adherence of SA to host tissues is mediated by a family of adhesins termed MSCRAMMs (microbial surface components recognizing adhesive matrix molecules), and expression of MSCRAMMs appears to be necessary for colonization of different tissues (8). The SA Map (MHC class II analog protein) protein, also referred to as EAP and p70, is a secreted protein that can bind to a variety of ECM components, including fibronectin, fibrinogen, vitronectin, bone sialoprotein, and thrombospondin (9–18). Map-deficient SA, however, is not impaired in its adhesion to different ECM components, suggesting that other adhesins can mediate SA adherence to the ECM and that Map may serve functions other than that of an adhesin (19, 20). Map contains six repeated domains of 110 amino acids; each containing a 30-amino acid subdomain with similarity to a sequence in the peptide-binding groove of the MHC class II β chain of various mammals (21). This striking similarity between Map and MHC II molecules suggested the possibility that Map may posses the ability to affect T cell function.

Map has been demonstrated to induce immunoglobulin synthesis and the proliferation of blood mononuclear cells in addition to shifting T cell responses in a Th2 direction (12, 13, 20, 21). The effects of Map on T cell responses may play a critical role in SA survival since

Received for publication July 1, 2002, and accepted in revised form September 23, 2002.

Address correspondence to: Eric L. Brown, The Center for Extracellular Matrix Biology, Texas A&M University Health Science Center, Albert B. Alkek Institute of Biosciences and Technology, 2121 West Holcombe Boulevard, Suite 603, Houston, Texas 77030-7552, USA. Phone: (713) 677-7572; Fax: (713) 677-7576; E-mail: ebrown@ibt.tamu.edu.
Yuko J. Miyamoto's present address is: Department of Pharmacology, School of Medicine, University of North Carolina, Chapel Hill, North Carolina, USA.
Kirk W. McCrea's present address is: University of Michigan, School of Public Health, Ann Arbor, Michigan, USA.
Damien McDevitt's present address is: Microbiology Department, Glaxo-Smith-Kline Pharmaceuticals, Collegeville, Pennsylvania, USA.

Conflict of interest: The authors have declared that no conflict of interest exists.

Nonstandard abbreviations used: *Staphylococcus aureus* (SA); microbial surface components recognizing adhesive matrix molecules (MSCRAMMs); delayed-type hypersensitivity (DTH); temperature sensitive origin of replication (*ts ori*); decorin-binding protein A (DbpA); Lennox broth (LB); binding buffer (BB); inactive *B. burgdorferi* (iBb); antigen-presenting cells (APCs); 3-{4,5-Dimethylthizol-2-y}-2,5diphenyl-tetraxolium bromide (MTT); propidium iodide (PI); microbial immunomodulatory molecule (MIM); open-reading frames (ORF).

the induction of Th1 (cellular immunity) responses during the course of SA infections have been associated with bacterial clearance in mice (22). The role of T cells in protection against SA infections in humans is less well-defined. SA infections do not usually result in protective immunity, and individuals can be subjected to persistent and repeated staphylococcal infections (23–26). While SA infections affecting the skin appear to be exacerbated by strong Th1-type response, it is clear that cellular immunity is critical in orchestrating the clearance of systemic SA infections and in preventing reinfection with the same or similar pathogen(s) (27–31). The capacity of Map to inhibit or shift the T cell response in a Th2 direction may serve as an additional mechanism facilitating SA survival and persistence.

Recently, Map has been described as an anti-inflammatory agent with the capacity to interfere with the innate host defense systems by preventing neutrophil recruitment, primarily by interacting with ICAM-1 on endothelial cells (20). In the studies reported here, we demonstrate that Map can also interfere with acquired immunity in a chronic murine SA-infection model (32). We demonstrated that BALB/c mice infected with SA genetically manipulated to be deficient in Map (Map^-SA) had significantly reduced levels of arthritis and abscess formation (heart and kidneys) following reinfection with wild-type SA (Map^+SA) compared with mice infected and reinfected with Map^+SA or mice receiving a single inoculum of Map^+SA. Furthermore, when T cell–deficient nude mice (*nu/nu*) were used in SA infection studies, Map^-SA was only marginally less effective in causing arthritis and osteomyelitis compared with Map^+SA–infected nude mice. Conversely, infections of the genotype control mice (*nu/+*) with Map^+SA or Map^-SA, respectively, resulted in disease presentation similar to that observed in SA-infected BALB/c mice. Since Th1 responses appear to be important in the control of SA infections (22), we examined the ability of isolated native or recombinant Map to modulate the Th1-mediated delayed-type hypersensitivity (DTH) response in mice and the effects of recombinant Map on the proliferation of a Th1 cell line in vitro. These data suggest that Map is a virulence factor that may play a role in SA persistence and survival by altering T cell function in vivo; however, it is unclear if and how Map's homology to MHC II relates to its T cell inhibitory properties.

Methods

Mice. Specific pathogen-free (MTV^-) BALB/c, C3H/Hen, *nu/nu* (nude), and *nu/+* mice were purchased from Harlan Sprague Dawley (Indianapolis, Indiana, USA). The animals were maintained in facilities approved by the American Association for Accreditation of Laboratory Animal Care in accordance with current regulations and standards of the United States Department of Agriculture, Department of Health and Human Services, and NIH. All animal procedures were approved by the Institutional Animal Care and Use Committee. In the experiments reported here we used female mice that were 8–10 weeks old at the start of each experiment.

Construction of a SA strain Newman Map deletion mutant. An allelic-replacement mutagenesis strategy was adopted to replace the native *map* locus with a gene that encodes drug resistance in SA strain Newman. The *map* gene and its up- and downstream flanking sequences were cloned on two overlapping plasmids: pMap5 harboring 1.9 kb of the *map* gene and 3.3 kb of downstream sequence and pMap6 harboring 1 kb of the *map* gene and 1 kb of upstream sequence. These are pBluescript SK(+) plasmids containing gene fragments from the original lambda gt 11 library of SA strain FDA 574 (21). The 3.3-kb downstream sequence of *map* was PCR amplified using pMap5 as template and primers R1 (*NcoI*/*HincII*), 5′-TGACCATGGCGTCGACATTTGTAGAGATGT-3′ (2174–2202 bp) and F1 (T7 primer from pBluescript), 5′-AATACGACTCACTATAGG-3′. The PCR product was purified, digested with *KpnI*/*NcoI* and the 1.7-kb digestion product was gel purified and ligated into pMap6, which had been digested with *KpnI*/*NcoI* to remove the *map* sequence. The resulting plasmid pMap7 contained both flanking sequences and only 50 nucleotides of the *map* gene.

Plasmid pRN6680 was digested with *HincII*/*SmaI* and the *tmn*-Tc^R marker was blunt-end ligated into *HincII*-digested pMap7 to generate plasmid pMap8 (33). To construct a shuttle plasmid that would replicate in SA but had a temperature sensitive origin of replication (*ts ori*), plasmid pMap8 was ligated with the SA *ts ori* from pE194. This *ts ori* is on a 3.7-kb *PstI* fragment that had been cloned from pRN5101 into the *PstI* site in pBluescript. The *PstI* sites of this *ts ori* were filled in and ligated into the *SmaI* site of pMap8. The resulting plasmid was called pMap9. Plasmid pMap9 was introduced into SA strain RN4220 by electroporation and then plated on TSA containing 10 μg/ml tetracycline and incubated at 30°C (34, 35). The temperature sensitivity of plasmid pMap9 in RN4220 was confirmed. The growth of a culture at 40°C in the presence of 10 μg/ml of tetracycline selected for plasmid pMap9 loss and isolation of mutants where allelic-replacement had occurred. The D*map:tmn* mutation was then transferred from SA strain RN4220 into SA strain Newman by phage 85 transduction (36). The correct chromosomal mutations in both strains RN4220 and Newman were confirmed by Southern hybridization analysis using gene probes for both the *map* and *tmn* genes (data not shown). Western immunoblotting of proteins released from the cell surface of Newman wild-type and Newman D*map:tmn* cells with 1 M LiCl also confirmed that the mutant failed to express the Map protein (data not shown).

Expression and purification of recombinant proteins. A recombinant version of Map designated Map19, decorin-binding protein A (DbpA), Ace19 and Ace40, were expressed using the pQE vector (QIAGEN Inc., Chatsworth, California, USA) in *Escherichia coli* (JM101) (Stratagene, La Jolla, California, USA) harboring the corresponding plasmids (Table 1) (37–41). The

Table 1
Recombinant proteins

Protein	Relevant characteristics	Reference
Map19	30 kDa; recombinant His tag protein contains the first and second MHC II analog domains from *S. aureus* strain FDA574, potential MSCRAMM, and anti-inflammatory agent	(12–13, 20–21)
Ace40	40 kDA; recombinant His tag protein contains the minimal collagen-binding domain from *E. faecalis*, MSCRAMM	(39–40)
Ace19	19 kDa; recombinant His tag protein (40), Truncated form of Ace40 with no collagen-binding activity, MSCRAMM	
DbpA	20 kDa; recombinant His tag protein, Decorin-binding protein A from *B. burdorferi*, MSCRAMM	(41)

resulting proteins contain an N-terminal His tag that allowed for purification using metal ion-chelating chromatography. Map19 contains residues 50–237 encompassing the first and second MHC II analog subdomains and is derived from strain FDA574 (21). The amino acid sequence is 84% identical and 95% similar to that of Newman Map in this region (21). *E. coli* were grown at 37°C in Lennox broth (LB) containing the appropriate antibiotics until they reached an A_{600} of 0.6 (42). Isopropyl-β-D-thiogalactopyranoside (Life Technologies Inc., Gaithersburg, Maryland, USA) was added to a final concentration of 0.2 mM, and the cells were incubated at 37°C for an additional 4 hours. Cells from a 1-l culture were harvested by centrifugation, resuspended in 10 ml binding buffer (BB) (20 mM Tris HCl, 0.5 M NaCl, 15 mM imidazole, pH 8.0), and lysed in a French pressure cell at 11,000 pounds/inch^2 (41). The lysate was centrifuged at 40,000 *g* for 15 minutes and the supernatant filtered through a 0.45-μm filter. A 1-ml iminodiacetic acid Sepharose column (Sigma-Aldrich, St. Louis, Missouri, USA) was charged with 75 mM $NiCl_2 \cdot 6H_2O$ and equilibrated with BB. The filtered supernatant was applied to the column and washed with 10 volumes of BB, then 10 volumes of BB containing 60 mM imidazole. The bound proteins were eluted with BB containing 200 mM imidazole, dialyzed against PBS containing 10 mM EDTA, then dialyzed against PBS (41). Protein concentrations were determined by the bicinchoninic acid protein assay (Pierce Chemical Co., Rockford, Illinois, USA), and proteins were stored at -20°C until use.

Quantitation of SA and intravenous injections. Map$^+$SA and Map$^-$SA (strain Newman) were grown overnight in LB (Difco Laboratories, Detroit, Michigan, USA) media at 37°C with shaking and were used in all infection experiments. Five hundred microliters of this culture was used to inoculate 50 ml of fresh LB in a 250-ml Erlenmeyer flask. The new cultures were grown as above until the optical density reached 0.5 at 600 nm using a 1-cm quartz cuvette. Aliquots of each culture were quantified for colony-forming units. The remainder of each culture was washed three times in sterile PBS. The cultures, based on prior growth curve determinations, were diluted to approximately 2×10^7 CFU/ml. Mice were injected intravenously with 10^7 SA in 0.5 ml PBS and monitored for up to 8 weeks. At the conclusion of the experiment, mice were sacrificed and the joints were examined histologically for osteomyelitis and arthritis as described previously (43, 44). Briefly, histopathological examination of hematoxylin- and eosin-stained formalin-fixed hind tibiotarsal joints were scored according to the level of cellular infiltrate (primarily neutrophils) as follows: 0, no arthritis/osteomyelitis; 1, minimal or rare (<10% tissue involvement); 2, mild (10–20%); 3, frequent (20–50%); 4, severe (>50%) (43, 44). All sections were examined without knowledge of the infection status of the mouse.

Quantification of SA in tissues. Mice (four mice/group) were infected with Map$^-$SA or Map$^+$SA as described above. Mice were sacrificed at various time points after infection (0.5, 1, 2, and 4 days), and their blood, heart, kidneys, and tibiotarsal joints (devoid of skin) were collected. Blood was collected aseptically into sterile Vacutainer tubes containing sodium heparin (Becton Dickinson and Co., Franklin Lakes, New Jersey, USA) as described (43, 44). The heart and both kidneys were collected aseptically and homogenized under sterile conditions using a mortar and pestle. Both hind tibiotarsal joints were homogenized using a Brinkman PT 10/35 homogenizer under sterile conditions. All homogenized tissues were serially diluted in sterile PBS and inoculated onto 5% sheep blood agar plates to estimate the bacterial density for each tissue. Plates were incubated at 37°C, and the number of colonies were counted 24–48 hours later. No

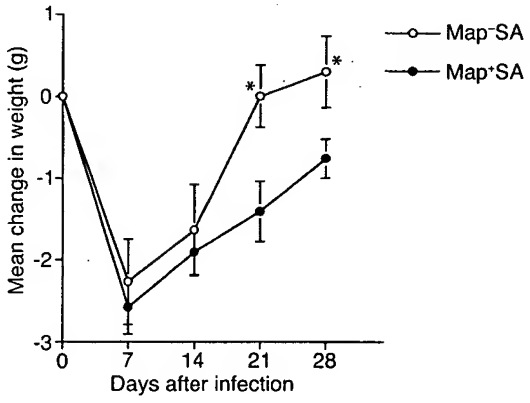

Figure 1
Mean weight loss from Map$^-$SA- and Map$^+$SA-infected mice. Mice were intravenously infected with either 10^7 Map$^-$SA or Map$^+$SA. Weights were taken before infection and every 7 days after infection for 4 weeks. Data are expressed as the mean ± SE of the mean of 26 and 24 mice/group for Map$^-$SA- and Map$^+$SA–infected mice, respectively. *$P < 0.05$, Student *t* test.

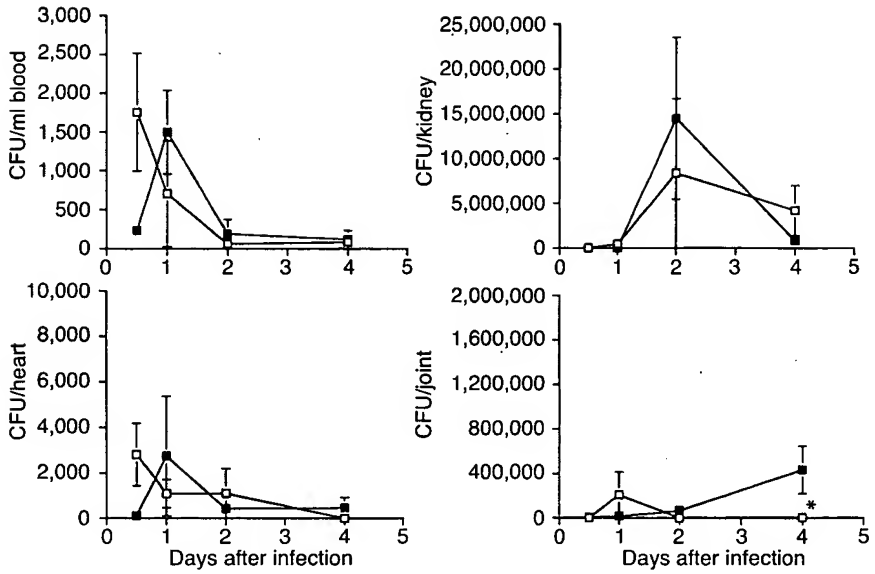

Figure 2
The number of bacteria isolated from various tissues. CFUs from blood, heart, kidneys, and joints were determined from mice infected with either Map⁻SA (open squares) or Map⁺SA (filled squares) at various times after infection. Data are expressed as the mean CFU ± SE of the mean of 4 mice/group at each time point. There was no statistical differences between infection groups at any of the time points examined (Student *t* test). *The bacterial density in the joints harvested from Map⁻SA–infected mice 4 days after infection was 5,750 ± 2,453.

bacterial colonies were detected in tissues harvested and cultured from uninfected mice.

Extraction of Map from SA. Map⁺SA and Map⁻SA were grown overnight as described above. Bacteria were pelleted by centrifugation and resuspended in 1 M LiCl (one-tenth of the original media volume). The suspension was incubated at 42°C with shaking for 2 hours. The bacteria were pelleted and the supernatant containing noncovalently attached surface proteins was removed and quantified for protein by determining the A_{280} using 1 M LiCl as a blank. Extracted proteins were diluted to 0.2 mg/ml in PBS and passed through a 0.22-μm filter for sterilization prior to intraperitoneal injection (45).

DTH assay. Mice were immunized with 20 μg of DbpA in CFA (Sigma-Aldrich) (day 0) (44). Seven days after immunization, mice were challenged in the hind footpads with 2.5 μg DbpA (50 μl PBS) (44). At the time of immunization, days 2, 4, and 6 after immunization, mice were injected intraperitoneally with 100 μg of native Map extracted from Map⁺SA, supernatant from Map⁻SA, or with various concentrations (1–500 μg) of the recombinant proteins Map19, Ace19, or Ace40 in 500 μl of PBS (38, 39, 41, 46–48). The footpads were measured before challenge and 24 hours later, using a spring-loaded micrometer (Mitutoyo, Tokyo, Japan). Mice were anesthetized with Isoflurane during footpad measurements (49).

Adoptive T cell transfer. BALB/c mice (five mice/group) were immunized with DbpA and were treated with recombinant Map19 or recombinant Ace40 as described above. The day after the last Map19 or Ace40 treatment, mice were sacrificed, and the spleens from each treatment group were enriched for T cells by passage over nylon wool columns as described previously (50). Twenty-four hours after intraperitoneal injection

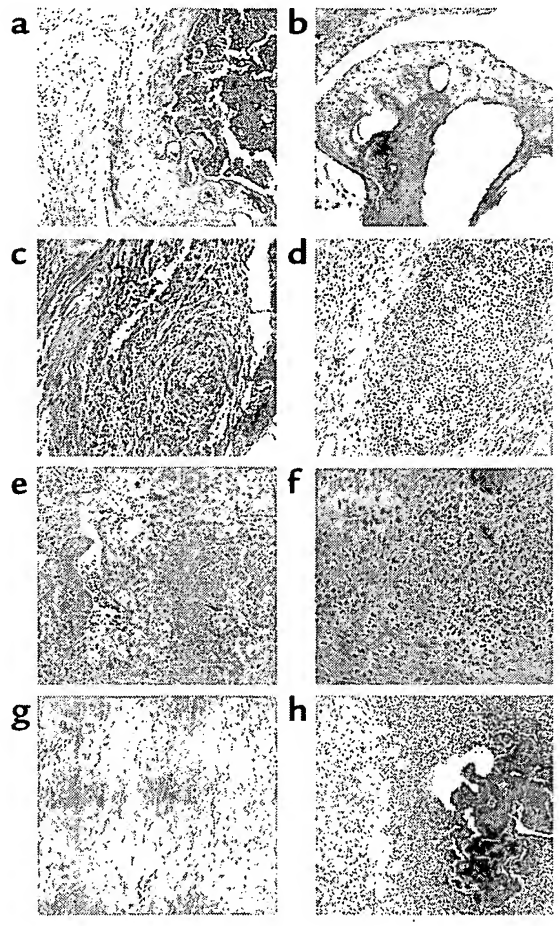

Figure 3
Hematoxylin- and eosin-stained tissue sections from Map⁻SA– or Map⁺SA–infected mice. (**a**) Severe osteomyelitis (BALB/c mouse infected with Map⁺SA). (**b**) No arthritis or osteomyelitis (BALB/c mouse infected with Map⁻SA). (**c–d**) Severe arthritis (*nu/nu* and *nu/+* mice infected with either Map⁻SA or Map⁺SA, respectively). (**e–f**) Kidney sections (BALB/c mice infected with Map⁻SA or Map⁺SA, respectively) and (**g–h**) heart sections (BALB/c mice infected with Map⁻SA or Map⁺SA, respectively).

Table 2
Histological examination of joints and abscess formation assessment in heart and kidneys harvested from Map$^-$SA- and Map$^+$SA-infected mice

Infecting strains	Mean arthritis score	Arthritis frequency(%)	Mean osteomyelitis score	Osteomyelitis frequency (%)
Map$^+$[A]	1.93 ± 0.38[B]	13/14 (93%)[C]	2.86 ± 0.40[D]	12/14 (86%)[E]
Map$^-$[A]	0.93 ± 0.28	8/16 (50%)	0.06 ± 0.06	1/16 (6%)
	Abscess formation (tissue examined)			
Infecting strains	Heart	Kidneys		
Map$^+$[A]	8/14 (57%)[F]	21/28 (75%)[F]		
Map$^-$[A]	0/16 (0%)	1/32 (3%)		

[A]BALB/c mice were infected intravenously with either 10^7 Map$^+$SA or Map$^-$SA strain Newman. Eight weeks later hind tibiotarsal joints were examined histologically for arthritis and hearts and kidneys were examined grossly and histologically for abscess formation. [B]$P < 0.05$ versus Map$^{-/-}$ 8-week group; Student t test. [C]$P < 0.05$ versus Map$^{-/-}$ 8-week group; Fisher's exact test. [D]$P < 0.0001$ versus Map$^{-/-}$ 8-week group; Student t test. [E]$P < 0.0001$ versus Map$^{-/-}$ 8-week group; Fisher's exact test. [F]$P < 0.0005$ versus Map$^{-/-}$ 8-week group; Fisher's exact test.

of T cells (10^7 nylon wool–enriched T cells/mouse in 500 μl of complete T lymphocyte media [CTL]), mice were challenged in the hind footpads with DbpA, and the DTH response was assessed as described above. CTL medium: RPMI-1640 containing 2 mM L-glutamine, 100 U/ml penicillin, 100 μg/ml streptomycin, 50 μg/ml gentamicin, 0.2 mM nonessential amino acids, 11 μg/ml sodium pyruvate, 0.02 M *N*-2-hydroxyethylpiperaxine-*N'*-2ethanesulfonic acid, and 5×10^{-5} N 2-mercaptoethanol plus 10% heat-inactivated FBS.

In vitro proliferation of BAT2.2 T cells. The *Borrelia burgdorferi*–specific mouse Th1 cell line BAT2.2 was stimulated with whole, inactive *B. burgdorferi* (iBb) and syngeneic (C3H/Hen) antigen-presenting cells (APCs), as described previously (43, 50). Briefly, 10^5 BAT2.2 T cells were cultured in 96-well flat-bottom plates (Corning-Costar Corp., Cambridge, Massachusetts, USA) along with 3×10^5 mitomycin-treated APCs in CTL medium and *Borrelia* (2 μg) in the presence of various proteins. Each treatment group was done in triplicate in a final volume of 200 μl complete medium. Each protein (10, 50, and 100 μg) was added to each well, and the T cells were allowed to proliferate for 24–48 hours at 37°C. Four hours before the end of the proliferation period, 20 μl/well of 3-{4,5-Dimethylthizol-2-y}-2,5diphenyl-tetraxolium bromide (MTT) (5 mg/ml; Sigma-Aldrich) was added to each well. After 4 hours of incubation at 37°C, 100 μl of solubilization buffer (0.04 N HCL in isopropanol) was added to each well and absorbance measured at 590 nm. Data are expressed as mean plus or minus SE of the mean of triplicate wells.

Assessment of Map-induced apoptosis of BAT2.2 cells. BAT2.2 T cells (10^6/well; 5 U IL-2/ml) were incubated in the presence of Map19 or Ace19 in a final volume of 1.5 ml complete media and examined for apoptosis using an Apoptotic DNA Ladder Kit (Roche Molecular Biochemicals, Indianapolis, Indiana, USA), according to the manufacturer's instructions. Two hundred micrograms of each protein was used and apoptosis measured after a 24-hour incubation at 37°C. Extracted DNA was treated with 10 μg/ml RNase (DNase free) for 1 hour at room temperature before examination by agarose gel electrophoresis.

Flow cytometry. T cells isolated for adoptive transfer experiments were nylon wool–enriched as described previously and examined by flow cytometric analysis to verify purity (50). Cells were washed in PBS containing 3% FBS (FACS buffer) and stained with the following mAb's: FITC-conjugated anti-mouse CD8a (Ly2) and

Table 3
Histological examination of joints and abscess formation assessment in heart and kidneys harvested from Map$^-$SA- and Map$^+$SA-infected mice reinfected with Map$^+$SA

Infecting strains	Mean arthritis score	Arthritis frequency (%)	Mean osteomyelitis score	Osteomyelitis frequency (%)
Map$^-$/Map$^+$[A,B]	0.84 ± 0.18[C]	14/26 (54%)[D]	0.57 ± 0.23[C]	6/26[E] (23%)
Map$^+$/Map$^+$[A,B]	1.65 ± 0.27	18/21 (86%)	1.95 ± 0.37	14/21 (66%)
-/Map$^+$[A,B]	2.06 ± 0.26	28/32 (88%)	1.48 ± 0.31	14/32 (44%)
	Abscess formation (tissue examined)			
Infecting strains	Heart	Kidneys		
Map$^-$/Map$^+$[A,B]	12/26 (46%)[F,G]	13/52 (25%)[H]		
Map$^+$/Map$^+$[A,B]	17/19 (89%)	33/38 (86%)		
-/Map$^+$[A,B]	29/31(94%)	48/62 (77%)		

[A]BALB/c mice were infected intravenously with either 10^7 Map$^+$ or Map$^-$SA strain Newman or left untreated. Four weeks after primary infection, mice from all groups received 10^7 Map$^+$SA intravenously. Four weeks later, the right hind-limb joint was harvested and examined histologically for arthritis and osteomyelitis. In addition, hearts and kidneys were examined grossly and histologically for abscess formation. [B]The data are pooled observations from three separate experiments. [C]$P < 0.005$ versus Map$^+$/Map$^+$ group; Students t test. [D]$P < 0.0001$ versus -/Map$^+$; Fisher's exact test. [E]$P < 0.0001$ versus Map$^+$/Map$^+$ and -Map$^+$ groups; Fisher's exact test. [F]$P < 0.005$ versus Map$^+$/Map$^+$ group; Fisher's exact test. [G]$P < 0.0001$ versus -/Map$^+$; Fisher's exact test versus -/Map$^+$; Fisher's exact test. [H]$P < 0.0001$ versus Map$^+$/Map$^+$ and -Map$^+$ groups; Fisher's exact test.

Table 4
Histological examination of joints harvested from Map⁻SA- or Map⁺SA-infected nude mice[A]

Infecting strains	Mean arthritis score	Arthritis frequency(%)	Mean osteomyelitis score	Osteomyelitis frequency (%)
nu/+/Map⁺SA	3.00 ± 0.24[B]	16/16 (100%)	3.19 ± 0.36[D,E]	14/16 (88%)
nu/+/Map⁻SA	1.78 ± 0.21	21/23 (91%)	0.34 ± 0.15	5/23 (22%)[G]
nu/nu/Map⁺SA	2.58 ± 0.25	12/12 (100%)	3.00 ± 0.32	12/12 (100%)
nu/nu/Map⁻SA	2.50 ± 0.26[C]	21/24 (88%)	1.58 ± 0.20[F]	15/24 (63%)

[A]Hsd *nu/nu* and *nu/+* mice were infected intravenously with either 10^7 Map⁻SA or Map⁺SA strain Newman or left untreated. Four weeks after primary infection, mice from all groups received 10^7 Map⁺SA intravenously. Four weeks later, the right hind-limb joint was harvested and examined histologically for arthritis and osteomyelitis. The data are pooled observations from two separate experiments. [B]$P < 0.005$ versus *nu/+*/Map⁻SA; Student *t* test. [C]$P < 0.05$ versus *nu/+* Map⁻SA group; Student *t* test. [D]$P < 0.0001$ versus *nu/+* Map⁻SA group; Student *t* test. [E]$P < 0.001$ versus *nu/nu* Map⁻SA group; Student *t* test. [F]$P < 0.001$ versus *nu/+* Map⁻SA group; Student *t* test. [G]$P < 0.05$ versus all groups; Fisher's exact test.

phycoerythrin-conjugated anti-mouse CD4 (L3T4) (PharMingen, San Diego, California, USA). The cells were incubated with the directly conjugated Ab's for 1 hour at 4°C and then washed with cold FACS buffer prior to FACS analysis. Annexin V-FITC (PharMingen) and propidium iodide (PI) (Sigma-Aldrich) staining of 10^6 BAT2.2 cells (5 U IL-2/ml) was performed 24 hours after incubation with either Map19 or DbpA (0.2 μg/μl) or left untreated in CTL media (2 ml), according to manufacturer's instructions. Cells from all groups were washed in cold FACS buffer and then analyzed on a Coulter EpicProfile flow cytometer (Coulter Corp., Miami, Florida, USA).

Results

Experimental SA infection. Mice challenged with a sublethal dose of virulent SA can develop severe arthritis and osteomyelitis in addition to abscesses in the heart and kidneys (32). To explore the role that Map might play in the pathogenesis of SA infections, BALB/c mice were infected with either 10^7 Map⁻SA or Map⁺SA strain Newman. During the initial stages of the infection, the groups of animals inoculated with the two strains were similarly affected, as indicated by recorded weight losses (Figure 1). The mean weight loss recorded for Map⁻SA- and Map⁺SA-infected mice 7 days after infection was −2.27 ± 0.52 and −2.58 ± 0.32 g, respectively; however, by day 21 after infection, the weight of Map⁻SA-infected mice returned to postinfection levels compared with Map⁺SA-infected mice, which were an average of 1.41 ± 0.37 g below preinfection weight readings (Figure 1). Furthermore, bacterial densities between infection groups were indistinguishable during the early stages of infection (Figure 2), suggesting that there were no differences in the capacity of Map⁻SA to colonize tissues when compared with Map⁺SA colonization.

Eight weeks after infection, 12 of 14 (86%) Map⁺SA-infected mice developed osteomyelitis, but only 1 of 16 (6%) Map⁻SA-infected mice was diagnosed with a bone infection (Figure 3, a and b, and Table 2). Arthritis frequency and severity were also significantly greater in Map⁺SA-infected mice compared with Map⁻SA-infected counterparts (Table 2). Furthermore, 8 of 14 (57%) Map⁺SA-infected mice developed heart abscesses and 21 of 28 (75%) kidneys examined were similarly affected (Figure 3, f and h, and Table 2). Conversely, none of the 16 Map⁻SA-infected mice developed heart abscesses and only 1 of 32 (3%) kidneys presented with an abscess (Figure 3, e and g, and Table 2). Taken together, these results demonstrated that the Map⁻SA strain was significantly less virulent in our animal model when compared with the parental Map⁺SA strain, suggesting that Map may be a virulence factor in chronic SA infections. Based on the sequence similarities with MHC class II molecules, we speculated that Map might act as an immunomodulator and that the observed differences between the Map⁺SA and Map⁻SA strains were due to suppressed host defenses in Map⁺SA-infected mice.

This hypothesis was tested in several experiments. First, mice were infected with either 10^7 Map⁺SA, Map⁻SA, or left untreated. Four weeks later, mice from all groups were reinfected with 10^7 Map⁺SA organisms. After an additional 4 weeks, mice from all groups were sacrificed and examined as described above. The results from these experiments suggested that mice initially infected with Map⁻SA were partially protected against the subsequent Map⁺SA challenge infection. These mice presented with

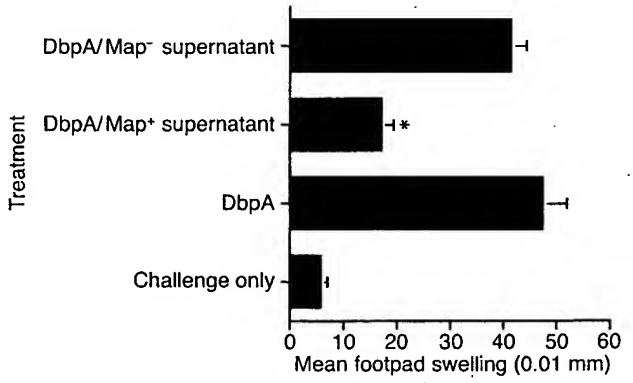

Figure 4
Native Map-mediated inhibition of DTH. DbpA-immunized mice were treated with native Map on the day of immunization (day 0) and on days 2, 4, and 6 after immunization. On day 7, mice were challenged with DbpA, and footpads were measured 0 and 24 hours after challenge. Mice treated with supernatant from Map⁺SA had a significantly reduced DTH response compared with immunized and challenged mice (*$P < 0.0001$; Student *t* test). Data are expressed as the mean ± SE of five mice.

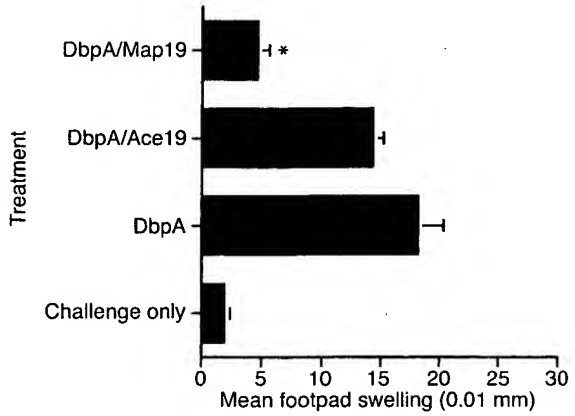

Figure 5
Recombinant Map19-mediated inhibition of DTH. DbpA-immunized mice were treated with recombinant Map19 on the day of immunization (day 0) and on days 2, 4, and 6 after immunization. On day 7, mice were challenged with DbpA and footpads were measured 0 and 24 hours after challenge. Mice treated with recombinant Map19 had a significantly reduced DTH response compared with immunized and challenged mice (*$P < 0.0001$; Student t test). Data are expressed as the mean ± SE of five mice.

significantly fewer heart (46%) and kidney (25%) abscesses following Map$^+$SA challenge compared with more than 75% abscess formation in hearts and kidneys from Map$^+$SA–infected and challenged mice or mice infected with a single dose of Map$^+$SA (i.e., –/Map+) (Table 3). Arthritis and osteomyelitis incidence and severity were also significantly reduced in Map$^-$SA–infected mice challenged with Map$^+$SA compared with control mice (Table 3). One possible explanation for these data is that Map$^-$SA–infected mice were capable of clearing the infection since their cellular responses were not impaired by Map while concomitantly establishing a memory response capable of clearing the second infection of Map$^+$SA. If Map functioned to impair T cell–mediated immunity, then mice initially infected with Map$^+$SA never fully cleared the infection and were likely not to have been able to develop a memory response capable of recognizing a second SA infection.

SA-infected nude mice. T cell–deficient nude (*nu/nu*) and genotype control (*nu/+*) mice were used to further assess the connection between SA virulence, Map, and T cell immunity. If Map is an immunomodulator with T cell inhibitory activities that facilitate SA survival and persistence, then Map$^-$SA–infected *nu/nu* mice should present with similar disease as Map$^+$SA–infected *nu/+* mice. Map$^-$SA-infected *nu/nu* mice had significantly higher arthritis and osteomyelitis scores compared with *nu/+*Map$^-$SA–infected mice. Furthermore, the arthritis scores between *nu/nu*/Map$^-$SA- and *nu/+*/Map$^+$SA–infected mice were similar (Figure 3, c and d, and Table 4), even though *nu/+*/Map$^+$SA–infected mice presented with significantly higher osteomyelitis scores (Table 4). Abscess formation was observed in all Map$^+$SA-infected mice but not in mice infected with Map$^-$SA, regardless of genotype. These data suggested that (a) the presence of Map on SA can affect the severity of arthritis and osteomyelitis through a T cell–mediated mechanism, and (b) Map plays a role in abscess formation through a T cell–independent mechanism(s).

Map-mediated inhibition of DTH. A direct in vivo assay for cellular immunity was used to assess the ability of Map to interfere with DTH. DTH responses are initiated and mediated by Th1 CD4$^+$ T cells in response to recall antigens, and these responses result in specific, measurable inflammation at the site of challenge. Mice immunized with a recombinant form of the *B. burgdorferi* MSCRAMM, DbpA, emulsified in CFA developed a significant DTH response to DbpA as measured by footpad swelling 7 days after immunization (Figure 4 and 5) (41, 44). Mice treated with native Map (Map$^+$SA supernatant), however, on the day of immunization (day 0) and days 2, 4, and 6 after immunization had a significantly reduced DTH response to DbpA challenge compared with untreated but immunized control mice and to mice treated with supernatants from Map$^-$SA (Figure 4). Similarly, mice treated with a recombinant form of Map (Map19) had a significantly reduced DTH response following DbpA challenge compared with untreated but immunized controls or the recombinant control protein Ace19–treated mice (Figure 5). Recombinant Map19 inhibited the DTH response in both BALB/c and C3H/Hen mice following immunization and challenge, demonstrating that Map has inhibitory affects not specific to particular mouse strains (Figure 5 and data not shown, respectively). The effects of Map19 were largely dose dependent with concentrations of 25 μg/mouse exhibiting significant inhibitory effects (Figure 6).

Adoptively transferred T cells from Map19-treated mice. Since adoptively transferred immune T cells confer immunity in syngeneic recipient mice, a cell transfer model was used to further dissect the cellular events underlying Map-mediated inhibition of DTH. Mice

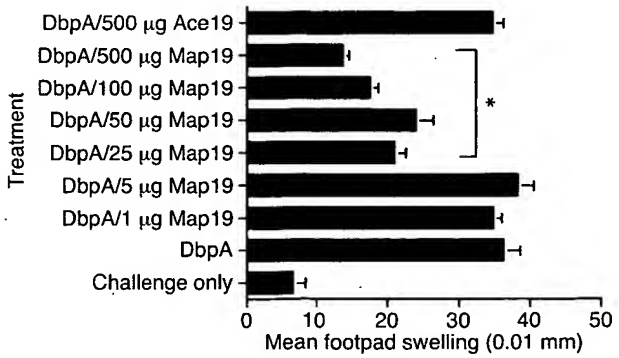

Figure 6
Dose-dependent inhibition of DTH. DbpA-immunized mice were treated with various doses of Map19 (1–500 μg) or Ace19 (500 μg), as described previously. On day 7, mice were challenged with DbpA, and the footpads measured 0 and 24 hours after challenge. Significant values are indicated by an asterisk ($P < 0.05$; Student t test). Data are expressed as the mean ± SE of five mice.

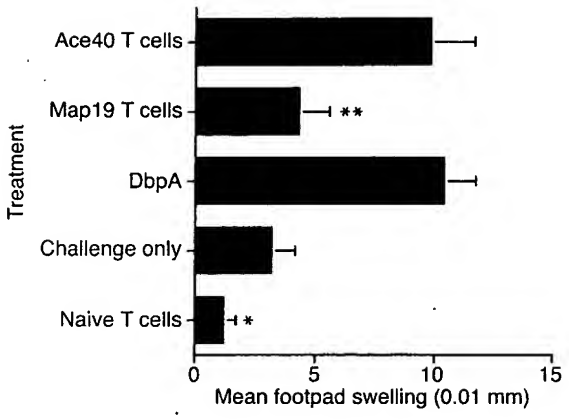

Figure 7
DTH following adoptive T cell transfer. DbpA-immunized mice were treated with either Map19 or Ace40, as described above. On day 7, mice were sacrificed and spleens were harvested and enriched for T cells by nylon wool purification. Cells (5×10^7) were injected intraperitoneally into syngeneic recipients. Twenty-four hours later, recipient mice were challenged with DbpA, and the DTH response was assessed as described above. T cells from DbpA-immunized Ace40-treated or T cells from DbpA-immunized (untreated) mice elicited a significant DTH response compared with unimmunized but challenged mice or to naive T cell–recipient mice (*$P < 0.04$; Student *t* test). T cells from DbpA-immunized, Map19-treated mice did not elicit a significant DTH response compared with positive control treatment groups (**$P < 0.001$; Student *t* test). Data are expressed as the mean ± SE of five mice.

immunized with DbpA were either left untreated or injected intraperitoneally with either Map19 or the recombinant control protein Ace40 on the day of immunization (day 0) and on days 2, 4, and 6 after immunization. On day 7, mice were sacrificed, and single cell suspensions from whole spleens were prepared and enriched for T cells by passage over nylon wool columns (50). Adoptive transfer of nylon wool–purified T cells from Map19-treated mice did not elicit a DTH response to DbpA in naive recipients compared with mice adoptively transferred with enriched T cells from Ace40-treated mice or untreated immune T cell control groups (Figure 7). Flow cytometric analysis of nylon wool–collected cells revealed a profile that was 46.83% ± 0.92% $CD4^+$, 31.63% ± 0.96% $CD8^+$, 1.2% ± 0.26% $CD4^+CD8^+$, and 20.4% ± 1.33% $CD4^-CD8^-$. These data are expressed as the mean percentage of positive cells plus or minus SE for the three groups examined.

Inhibition of T cell proliferation and apoptosis assessment. Recombinant Map19 and Ace19 were tested for their ability to inhibit the proliferation of the *Borrelia*-specific T cell line BAT 2.2 (43, 50). T cell proliferation was measured 48 hours after plating in the presence of mitomycin C–treated syngeneic APCs and iBb (50). Proliferation was measured as a function of tetrazolium blue production following a 4-hour incubation in the presence of MTT. Map19-treated BAT 2.2 cells were inhibited significantly from proliferating (Figure 8). Map19 did not inhibit BAT2.2 proliferation if the APCs were preincubated in the presence of either Map19 or Ace19 for 6 hours and then washed prior to the addition of iBb and BAT2.2 cells, suggesting Map had its inhibitory effects on T cells (data not shown). Furthermore, APCs preincubated with Map19 and iBb for 6 hours induced BAT2.2 proliferation, suggesting that Map did not affect the ability of the APCs to process antigen (data not shown).

Microscopic analysis of BAT2.2 cells cultured in the presence of Map19 revealed significant morphological changes (e.g., cell shrinkage) compared with untreated cells or cells cultured in the presence of control proteins (data not shown), suggesting that apoptosis or necrosis but not anergy were likely induced by Map. FACS analysis of BAT2.2 cells stained with annexin V-FITC and PI revealed that 76% of BAT2.2 Map19-treated cells (Figure 9c) were both annexin V-FITC/PI positive compared with almost 11% double-positive cells for both untreated and DbpA-treated cells (Figure 9, a and b, respectively). FACS analysis at earlier time points did not reveal significant differences between treatment groups (data not shown). Since cells that have already undergone an apoptotic death will eventually also stain positive for PI, it was not possible to distinguish if Map-treated cells in this assay were in a state of late apoptosis or necrosis (51). To differentiate between these forms of cell death, DNA extracted from BAT2.2 T cells incubated in the presence of Map19 was examined for fragmentation by gel electrophoresis (Figure 10). DNA extracted from Map19-treated cells (lane 3) was fragmented comparable to the apoptotic-positive control DNA (lane 5) but not DNA extracted from untreated (lane 2) or Ace40-treated (lane 4) T cells (Figure 10), suggesting that Map can, at least in vitro, prevent T cell function by induction of apoptosis.

Discussion

Mechanisms of immune escape are used by many infectious agents affecting humans. The nature of these strategies significantly vary and can be classified into various categories: the generation of physical barriers (biofilm

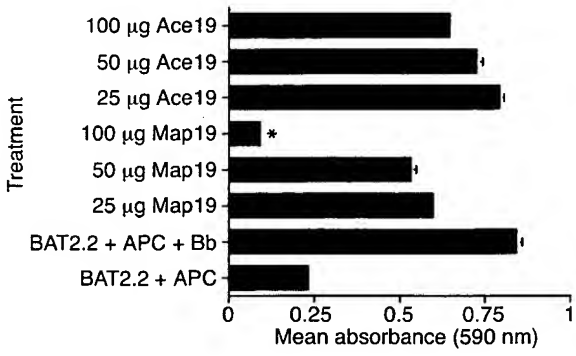

Figure 8
Map-induced inhibition of T cell proliferation. BAT2.2 T cell proliferation was measured after 48 hours in culture in the presence of APCs, and antigen in the presence of Map 19 or Acel9 at various concentrations. *$P < 0.0001$ compared with all other treatment groups; Student *t* test. Data are expressed as the mean absorbance ± SE of triplicate wells.

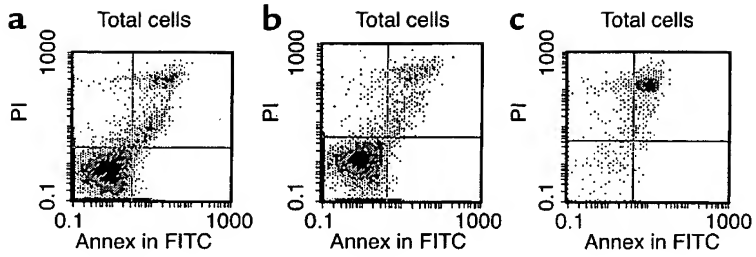

Figure 9
The effect of Map19 on annexin V/PI staining. BAT2.2 cells (10^6) (5 U IL-2/ml) were incubated in media alone (**a**) or in the presence of either 400 μg of either Ace40 (**b**) or Map19 (**c**) for 24 hours and analyzed by FACS following incubations with annexin V-FITC and PI.

formation) that protect bacteria against immune attack (52, 53); the secretion of immunoregulatory cytokine analogs or the induction of host cytokines that potentiate nonprotective immunity, resulting in pathogen survival (54–58); antigenic variation, which can prevent the generation of a protective immune response (59–61); antigenic mimicry, which can result in either immune modulation (e.g., MHC I analogs) or sequestration of the pathogen from the immune system (62, 63); toxin and protease production, which can destroy different cell types, including immune cells (2, 52); and finally, direct modulation of host cell functions, which can result in the induction or inhibition of apoptosis, respectively, depending on the pathogen (64–69).

Reinfection of humans with SA is one of the hallmarks of diseases caused by this pathogen, and a difficulty in clearing these types of infections is not only a function of disseminated disease but of SA immune escape mechanisms (23–26). One possible reason for recurring infections is that leukocytes from patients with chronic or recurrent SA infections have impaired chemotactic, phagocytic, and bactericidal functions (25, 30, 31). Whether these defects in lymphocyte function were a result of the bacterial infection or a preexisting condition in these individuals is not known (25, 30, 31). More specifically, superantigens and protein A produced by SA during an infection serve immune-evasion functions that may potentiate ongoing and recurrent infections (2).

Here we describe a third SA MIM (microbial immunomodulatory molecule) with potential T cell–limiting properties. The first observation suggesting Map acted in this capacity stemmed from double infection studies in which a primary infection with Map$^-$SA conferred significant protection against reinfection with Map$^+$SA. This contrasted significantly with the pathologies observed in mice receiving primary and secondary Map$^+$SA infections. One explanation for these data is that T cell–mediated responses in Map$^+$SA-infected mice were abrogated by the presence of Map. In contrast, Map$^-$SA-infected mice developed cell-mediated immunity over the course of infection, resulting in bacterial clearance and in a memory response capable of controlling a secondary Map$^+$SA infection. That a primary Map$^-$SA infection conferred significant but incomplete protection against Map$^+$SA challenge suggested that the balance or competition between an anamnestic response and Map-mediated immunomodulation could be affected by the challenge dose. Although these data suggested that Map acted as an immunoregulatory molecule, we could not exclude the following two possibilities: first, if Map is a critical adhesin required during the infection process, its removal may have resulted in an attenuated SA strain that served to "vaccinate" mice against the second Map$^+$SA infection. This is not a likely scenario since Map-deficient SA still efficiently adhere to individual ECM molecules (19, 20). Furthermore, the mean weight loss between Map$^-$SA– and Map$^+$SA–infected mice was similar during the first weeks after infection, and the bacterial densities in various tissues were indistinguishable between infection groups, suggesting that bacterial adhesion, a critical early step during infection, was not compromised in Map$^-$SA. This weight-loss pattern is significantly different from that recorded for mice infected with SA deficient in the collagen-binding protein CNA (CNA-SA). Weight loss differences in these animals, compared with CNA$^+$SA–infected controls diverged from the start of the infection process (E.L. Brown et al., unpublished observations). Second, a diminished disease state following Map$^-$SA infection may have been a result of polar effects caused by *map* inactivation following transformation resulting in the inactivation of other genes required for SA survival or virulence. Although a *map*-complemented Map$^-$SA strain Newman is not yet available, the significant effects of both isolated native Map

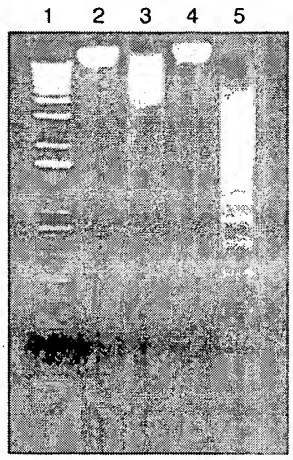

Figure 10
Map-induced apoptosis of BAT2.2 T cells. BAT2.2 cells (2×10^6) (5 U IL-2/ml) were incubated in media alone (lane 2) or in the presence of either 100 μg Map19 (lane 3) or Ace40 (lane 4). DNA from U937 cells were used as a positive control (lane 5). Lane 1, 100-bp ladder.

and of recombinant Map19 on cellular immunity strongly suggested that the lack of virulence observed for Map$^-$SA was a function of the bacteria's inability to affect host immunity and not a result of the *map* inactivation process. In addition, *nu/nu* mice infected with Map$^-$SA presented with more severe arthritis compared with *nu/+* mice infected with Map$^-$SA. Interestingly, abscess formation was absent in *nu/nu* and *nu/+* Map-SA–infected mice but not in Map$^+$SA–infected mice of either genotype. These data suggested a potential role for T cells in controlling joint pathology but not in protection against abscess formation. These experiments somewhat contradict findings in a rat model that suggested that T cells are critical for abscess formation and with recent work describing Map as an anti-inflammatory agent in a mouse peritonitis model (20, 70). However, both of these studies examined acute SA infections in contrast to the assessment of chronic disease described here. Furthermore, the infection routes (intraperitoneal) and the parameters used to assess disease were significantly different in both studies (20, 70). These differences make it difficult to reconcile the anti-inflammatory effects of Map described in a thioglycollate-induced peritonitis model with the abscesses and severe joint disease caused by a chronic SA infection (20).

Additional evidence suggesting that Map affected T cell function stemmed from experiments demonstrating that Map inhibited DTH responses and induced T cell death in vitro most likely by apoptosis. The effects of Map on T cell function appeared only to affect mature T cells stimulated in the context of antigen and MHC II. It is interesting to speculate that this effect of Map on T cells is a function of the homology between Map and MHC class II molecules since the proliferation of naive T cells following incubation with concanavalin A or by Ab cross-linking of the T cell receptor was not inhibited by Map19 (McIntyre and Miyamoto, unpublished observations). Interference of Map with the interactions between activated T cells and MHC class II–bearing APCs may explain why Map only affected T cell proliferation in the context of antigen and APCs. Furthermore, a human T cell line cultured in the presence of plate-bound fibronectin and αCD3 proliferated in the presence of Map19 (B.W. McIntyre and Y.J. Miyamoto, unpublished observations). These data suggested that activated T cells, but not naive T cells, were susceptible to inhibition of proliferation by Map and that T cell lines induced to proliferate via "non-classical" pathways bypassed Map-mediated mechanisms that resulted in the loss of T cell function.

Sequence analysis of the SA genome revealed four open-reading frames (ORFs) encoding Map-like proteins in meticillin-resistant SA strain N315 (38). The ORF designated SA1751 encodes a protein with a 69% identity to Map from strain FDA574 (21, 38). The SA1751 sequence is truncated by a stop codon immediately after an adenine-rich region, and expansion of this region by one adenine would remove the stop codon; the adjacent MHC II homologous region (SA1750) would be encoded (38). This suggested that SA can express longer or shorter forms of Map by modulating the length of the alanine repeat region (38). The remaining ORFs (SA2006 and SA0841) encode proteins with 34 and 44% identity, respectively, to the FDA574 Map protein. The role of these Map homologues in SA infection is unknown at this time. Perhaps the potential to encode a variety of MHC II–like proteins can serve to potentiate survival of various SA strains in mammals of varied genetic backgrounds. Extensive searches for Map homologues using the available public databases revealed no similar proteins in other bacteria.

SA uses various survival strategies that allow it to persist in mammalian hosts. Furthermore, persistent and recurrent SA infections point to mechanisms that obstruct the development of protective immunity. One of the functions of the Map protein suggested that it may function to impede the development and maintenance of memory responses. Apoptotic modulation by MIMs is just one mechanism of immune evasion used by human pathogens. Elucidation of the structure of this class of molecules, their functions, and mechanisms of action may be used to design strategies to prevent or treat disease.

Acknowledgments

This work was supported by the Department of Health and Human Services, grants from the Center for Disease Control (CCU618387) to E. Brown, by NIH grant AI-20624 to M. Höök and grant CA-62596 to B. McIntyre, and Cancer Immunobiology Training Program Grant CA09598 to Y. Miyamoto. We thank Andrew Spicer for critical review of the manuscript and Karen Ramirez for flow cytometry operation and technical assistance.

1. Kissane, J.M. 1997. Staphylococcal infections. In *Pathology of Infectious Diseases.* Vol. I. D.H. Connor, F.W. Chandler, H.J. Schwartz, H.J. Manz, and E.E. Lack, editors. Appleton and Lange. Stamford, Connecticut, USA. 805–816.
2. Lowy, F.D. 1998. *Staphylococcus aureus* infections. *N. Engl. J. Med.* **339**:520–532.
3. Rupp, M.E. 1997. Infections of intravascular catheters and vascular devices. In *The staphylococci in human disease.* K.B. Crossley and G.L. Archer, editors. Churchill Liningstone. New York, New York, USA. 379–399.
4. Tacconelli, E., Tumbarello, M., and Cauda, R. 1998. *Staphylococcus aureus* infections. *N. Engl. J. Med.* **339**:2026–2027.
5. Petros, S., et al. 1998. Severe community acquired pneumonia due to *Staphylococcus aureus. Intensive Care Med.* **24**:189.
6. Kim, H.S., Weilbaecher, D.G., Lie, J.T., and Titus, J.L. 1978. Myocardial abscesses. *Am. J. Clin. Pathol.* **70**:18–23.
7. Hiramatsu, K., Cui, L., Kuroda, M., and Ito, T 2001. The emergence and evolution of methicillin-resistant *Staphylococcus aureus. Trends Microbiol.* **9**:486–493.
8. Patti, J.M., Allen, B.L., McGavin, M.J., and Höök, M. 1994. MSCRAMM-mediated adherence of microorganisms to host tissues. *Annu. Rev. Microbiol.* **48**:585–617.
9. Herrmann, M., Suchard, S.J., Boxer, L.A., Waldvogel, F.A., and Lew, P.D. 1991. Thrombospondin binds to *Staphylococcus aureus* and promotes staphylococcal adherence to surfaces. *Infect. Immun.* **59**:279–288.
10. Fujigaki, Y., et al. 1998. Glomerular injury induced by cationic 70-kD staphylococcal protein; specific immune response is not involved in early phase in rats. *J. Pathol.* **184**:436–445.
11. Chhatwal, G.S., Preissner, K.T., Muller-Berghaus, G., and Blobel, H. 1987. Specific binding of the human S protein (vitronectin) to streptococci, *Staphylococcus aureus*, and *Escherichia coli. Infect. Immun.* **55**:1878–1883.
12. Jahreis, A., Beckheinrich, P., and Haustein, U.F. 2000. Effects of two novel cationic staphylococcal proteins (NP-tase and p70)and enterotoxin B on IgE synthesis and interleukin-4 and interferon-gamma production in patients with atopic dermatitis. *Br. J. Dermatol.* **142**:680–687.
13. Jahreis, A., et al. 1995. Two novel cationic staphylococcal proteins induce

IL-2 secretion, proliferation and immunoglobulin synthesis in peripheral blood mononuclear cells (PBMC) of both healthy controls and patients with common variable immunodeficiency (CVID). *Clin. Exp. Immunol.* **100**:406–411.
14. Hudson, M.C., Ramp, W.K., and Frankenburg, K.P. 1999. *Staphylococcus aureus* adhesion to bone matrix and bone-associated biomaterials. *FEMS Microbiol. Lett.* **173**:279–284.
15. Lopes, J.D., dos Reis, M., and Brentani, R.R. 1985. Presence of laminin receptors in *Staphylococcus aureus*. *Science.* **229**:275–277.
16. O'Connell, D.P., et al. 1998. The fibrinogen-binding MSCRAMM (clumping factor) of *Staphylococcus aureus* has a Ca^{2+}-dependent inhibitory site. *J. Biol. Chem.* **273**:6821–6829.
17. Vercellotti, G.M., et al. 1985. Extracellular matrix proteins (fibronectin, laminin, and type IV collagen) bind and aggregate bacteria. *Am. J. Pathol.* **120**:13–21.
18. Wann, E.R., Gurusiddappa, S., and Höök, M. 2000. The fibronectin-binding MSCRAMM FnbpA of *Staphylococcus aureus* is a bifunctional protein that also binds to fibrinogen. *J. Biol. Chem.* **275**:13863–13871.
19. Kreikemeyer, B., McDevitt, D., and Podbielski, A. 2002. The role of the Map protein in *S. aureus* matrix protein and eukaryotic cell adherence. *Int. J. Med. Microbiol.* **292**:283–295.
20. Chavakis, T., et al. 2002. *Staphylococcus aureus* extracellular adherence protein serves as anti- inflammatory factor by inhibiting the recruitment of host leukocytes. *Nat. Med.* **8**:687–693.
21. Jonsson, K., McDevitt, D., McGavin, M.H., Patti, J.M., and Höök, M. 1995. *Staphylococcus aureus* expresses a major histocompatibility complex class II analog. *J. Biol. Chem.* **270**:21457–21460.
22. Guillen, C., et al. 2002. Enhanced Th1 response to *Staphylococcus aureus* infection in human lactoferrin-transgenic mice. *J. Immunol.* **168**:3950–3957.
23. Chang, H.R., et al. 2000. Use of pulsed-field gel electrophoresis in the analysis of recurrent *Staphylococcus aureus* infections in patients on continuous ambulatory peritoneal dialysis. *Am. J. Nephrol.* **20**:463–467.
24. Hartstein, A.I., Mulligan, M.E., Morthland, V.H., and Kwok, R.Y. 1992. Recurrent *Staphylococcus aureus* bacteremia. *J. Clin. Microbiol.* **30**:670–674.
25. Monteil, M., Hobbs, J., and Citron, K. 1987. Selective immunodeficiency affecting staphylococcal response. *Lancet.* **2**:880–883.
26. Shayegani, M., De Courcy, S.J., Jr., and Mudd, S. 1973. Cell-mediated immunity in mice infected with *S. aureus* and elicited with specific bacterial antigens. *J. Reticuloendothel. Soc.* **14**:44–51.
27. Easmon, C.S., and Glynn, A.A. 1975. Cell-mediated immune responses in *Staphylococcus aureus* infections in mice. *Immunology.* **29**:75–85.
28. Ficker, L., Seal, D., and Wright, P. 1989. Staphylococcal infection and the limbus: study of the cell-mediated immune response. *Eye.* **3**:190–193.
29. Sarai, Y., et al. 1977. Immunological properties in staphylococcal toxic epidermal necrolysis. *Dermatologica.* **155**:315–318.
30. Verbrugh, H.A., et al. 1980. Phagocytic and chemotactic function of polymorphonuclear and mononuclear leucocytes in patients with recurrent staphylococcal infections. *Scand. J. Infect. Dis.* **12**:111–116.
31. Valmin, K., Hallberg, T., and Hedstrom, S.A. 1982. Recurrent *Staphylococcal furunculosis*: lymphocyte subsets and plasma immunoglobulins. *Scand. J. Infect. Dis.* **14**:153–154.
32. Bremell, T., Lange, S., Yacoub, A., Ryden, C., and Tarkowski, A. 1991. Experimental *Staphylococcus aureus* arthritis in mice. *Infect. Immun.* **59**:2615–2623.
33. Sloane, R., et al. 1991. A toxic shock syndrome toxin mutant of *Staphylococcus aureus* isolated by allelic replacement lacks virulence in a rabbit uterine model. *FEMS Microbiol. Lett.* **62**:239–244.
34. Hussain, M., et al. 2002. Insertional inactivation of Eap in *Staphylococcus aureus* strain Newman confers reduced staphylococcal binding to fibroblasts. *Infect. Immun.* **70**:2933–2940.
35. Kreiswirth, B.N., et al. 1983. The toxic shock syndrome exotoxin structural gene is not detectably transmitted by a prophage. *Nature.* **305**:709–712.
36. Duthie, E.S., and Lorenz, L.L. 1952. Staphylococcal coagulase: mode of action and antigenicity. *J. Gen. Microbiol.* **6**:95–107.
37. Ponnuraj, K., et al. 2002. Crystallization and preliminary x-ray crystallographic analysis of Ace: a collagen-binding MSCRAMM from *Enterococcus faecalis*. *Biochim. Biophys. Acta.* **1596**:173–176.
38. Kuroda, M., et al. 2001. Whole genome sequencing of meticillin-resistant *Staphylococcus aureus*. *Lancet.* **357**:1225–1240.
39. Visai, L., et al. 2000. Monoclonal antibodies to CNA, a collagen-binding microbial surface component recognizing adhesive matrix molecules, detach *Staphylococcus aureus* from a collagen substrate. *J. Biol. Chem.* **275**:39837–39845.
40. Rich, R.L., et al. 1999. Ace is a collagen-binding MSCRAMM from *Enterococcus faecalis*. *J. Biol. Chem.* **274**:26939–26945.
41. Guo, B.P., Brown, E.L., Dorward, D.W., Rosenberg, L.C., and Höök, M. 1998. Decorin-binding adhesins from *Borrelia burgdorferi*. *Mol. Microbiol.* **30**:711–723.
42. Maniatis, T., Fritsch, E.F., and Sambrook, J. 1989. *Molecular cloning: A laboratory manual*. Cold Spring Harbor Laboratory Press. Cold Spring Harbor, New York, USA. A.3
43. Brown, E.L., Ullrich, S.E., Pride, M., and Kripke, M.L. 2001. The effect of UV irradiation on infection of mice with *Borrelia burgdorferi*. *Photochem. Photobiol.* **73**:537–544.
44. Brown, E.L., et al. 2001. Resistance to Lyme disease in decorin-deficient mice. *J. Clin. Invest.* **107**:845–852.
45. McGavin, M.H., Krajewska-Pietrasik, D., Ryden, C., and Höök, M. 1993. Identification of a *Staphylococcus aureus* extracellular matrix-binding protein with broad specificity. *Infect. Immun.* **61**:2479–2485.
46. Patti, J.M., et al. 1994. The *Staphylococcus aureus* collagen adhesin is a virulence determinant in experimental septic arthritis. *Infect. Immun.* **62**:152–161.
47. Switalski, L.M., et al. 1993. A collagen receptor on *Staphylococcus aureus* strains isolated from patients with septic arthritis mediates adhesion to cartilage. *Mol. Microbiol.* **7**:99–107.
48. Joh, H.J., House-Pompeo, K., Patti, J.M., Gurusiddappa, S., and Höök, M. 1994. Fibronectin receptors from gram-positive bacteria: comparison of active sites. *Biochemistry.* **33**:6086–6092.
49. Brown, E.L., et al. 1995. Modulation of immunity to *Borrelia burgdorferi* by ultraviolet irradiation: differential effect on Th1 and Th2 immune responses. *Eur. J. Immunol.* **25**:3017–3022.
50. Pride, M.W., et al. 1998. Specific Th1 cell lines that confer protective immunity against experimental *Borrelia burgdorferi* infection in mice. *J. Leukoc. Biol.* **63**:542–549.
51. Vermes, I., Haanen, C., Steffens-Nakken, H., and Reutelingsperger, C. 1995. A novel assay for apoptosis. Flow cytometric detection of phosphatidylserine expression on early apoptotic cells using fluorescein labelled Annexin V. *J. Immunol. Methods.* **184**:39–51.
52. Kharazmi, A. 1991. Mechanisms involved in the evasion of the host defence by *Pseudomonas aeruginosa*. *Immunol. Lett.* **30**:201–205.
53. Martin-Lopez, J.V., et al. 2002. Detection of *Staphylococcus aureus* clinical isolates harboring the ica gene cluster needed for biofilm establishment. *J. Clin. Microbiol.* **40**:1569–1570.
54. Suzuki, T., et al. 1995. Viral interleukin 10 (IL-10), the human herpes virus 4 cellular IL-10 homologue, induces local anergy to allogeneic and syngeneic tumors. *J. Exp. Med.* **182**:477–486.
55. Engele, M., et al. 2002. Induction of TNF in human alveolar macrophages as a potential evasion mechanism of virulent *Mycobacterium tuberculosis*. *J. Immunol.* **168**:1328–1337.
56. de Diego, J., Punzon, C., Duarte, M., and Fresno, M. 1997. Alteration of macrophage function by a *Trypanosoma cruzi* membrane mucin. *J. Immunol.* **159**:4983–4989.
57. Abraham, S.N., Beachy, E.H., and Simpson, W.A. 1983. Adherence of streptococcus pyogenes, Escherichia coli, and Pseudomonas aeruginosa to fibronectin-coated and uncoated epithelial cells. *Infect. Immun.* **41**:1261–1268.
58. Akridge, R.E., Oyafuso, L.K., and Reed, S.G. 1994. IL-10 is induced during HIV-1 infection and is capable of decreasing viral replication in human macrophages. *J. Immunol.* **153**:5782–5789.
59. Donelson, J.E., Hill, K.L., and El-Sayed, N.M. 1998. Multiple mechanisms of immune evasion by African trypanosomes. *Mol. Biochem. Parasitol.* **91**:51–66.
60. Kyes, S., Horrocks, P., and Newbold, C. 2001. Antigenic variation at the infected red cell surface in malaria. *Annu. Rev. Microbiol.* **55**:673–707.
61. Lawrenz, M.B., et al. 1999. Human antibody responses to VlsE antigenic variation protein of *Borrelia burgdorferi*. *J. Clin. Microbiol.* **37**:3997–4004.
62. Wurzner, R. 1999. Evasion of pathogens by avoiding recognition or eradication by complement, in part via molecular mimicry. *Mol. Immunol.* **36**:249–260.
63. Farrell, H.E., et al. 1997. Inhibition of natural killer cells by a cytomegalovirus MHC class I homologue in vivo. *Nature.* **386**:510–514.
64. Boulton, I.C., and Gray-Owen, S.D. 2002. Neisserial binding to CEACAM1 arrests the activation and proliferation of CD4+ T lymphocytes. *Nat. Immunol.* **3**:229–236.
65. Cuff, S., and Ruby, J. 1996. Evasion of apoptosis by DNA viruses. *Immunol. Cell Biol.* **74**:527–537.
66. Das, G., Vohra, H., Saha, B., Agrewala, J.N., and Mishra, G.C. 1998. *Leishmania donovani* infection of a susceptible host results in apoptosis of Th1-like cells: rescue of anti-leishmanial CMI by providing Th1-specific bystander costimulation. *Microbiol. Immunol.* **42**:795–801.
67. Monack, D.M., Mecsas, J., Ghori, N., and Falkow, S. 1997. Yersinia signals macrophages to undergo apoptosis and YopJ is necessary for this cell death. *Proc. Natl. Acad. Sci. USA.* **94**:10385–10390.
68. Nunes, M.P., Andrade, R.M., Lopes, M.F., and DosReis, G.A. 1998. Activation-induced T cell death exacerbates *Trypanosoma cruzi* replication in macrophages cocultured with CD4+ T lymphocytes from infected hosts. *J. Immunol.* **160**:1313–1319.
69. Wei, S., et al. 2002. *Toxoplasma gondii*-infected human myeloid dendritic cells induce T-lymphocyte dysfunction and contact-dependent apoptosis. *Infect. Immun.* **70**:1750–1760.
70. Tzianabos, A.O., and Kasper, D.L. 2002. Role of T cells in abscess formation. *Curr. Opin. Microbiol.* **5**:92–96.

Suppression of experimental autoimmune encephalomyelitis by extracellular adherence protein of *Staphylococcus aureus*

Changping Xie,[2] Pilar Alcaide,[4] Brian V. Geisbrecht,[3] Darius Schneider,[2] Mathias Herrmann,[5] Klaus T. Preissner,[6] Francis W. Luscinskas,[4] and Triantafyllos Chavakis[1]

[1]Experimental Immunology Branch, National Cancer Institute, National Institutes of Health, Bethesda, MD 20892
[2]Department of Internal Medicine I, University Heidelberg, D-69120 Heidelberg, Germany
[3]Division of Cell Biology and Biophysics, School of Biological Sciences, University of Missouri-Kansas City, Kansas City, MO 64110
[4]Department of Pathology, Brigham and Women's Hospital, Harvard Medical School, Boston, MA 02115
[5]Institute of Medical Microbiology and Hygiene, University of Saarland Hospital, D-66421 Homburg/Saar, Germany
[6]Institute for Biochemistry, Medical School, Justus-Liebig-University, D-35392 Giessen, Germany

Multiple sclerosis (MS) is a devastating inflammatory disorder of the central nervous system (CNS). A major hallmark of MS is the infiltration of T cells reactive against myelin components. T cell infiltration is mediated by the interaction of integrins of the β1 and β2 family expressed by lymphocytes with their endothelial counter-receptors, vascular cell adhesion molecule 1 and intercellular adhesion molecule (ICAM)-1, respectively. We have reported previously that extracellular adherence protein (Eap) of *Staphylococcus aureus* exerts anti-inflammatory activities by interacting with ICAM-1 and blocking β2-integrin–dependent neutrophil recruitment. Here, we report that Eap inhibits experimental autoimmune encephalomyelitis (EAE) in mice. In vitro, Eap reduced adhesion of peripheral blood T cells to immobilized ICAM-1 as well as their adhesion and transmigration of TNF-activated human endothelium under static and shear flow conditions. These inhibitory effects were corroborated in two mouse models of inflammation. In a delayed-type hypersensitivity model, both T cell infiltration and the corresponding tissue edema were significantly reduced by Eap. In addition, Eap administration prevented the development of EAE and markedly decreased infiltration of inflammatory cells into the CNS. Strikingly, intervention with Eap after the onset of EAE suppressed the disease. Collectively, our findings indicate that Eap represents an attractive treatment for autoimmune neuroinflammatory disorders such as MS.

CORRESPONDENCE
Triantafyllos Chavakis:
chavakist@mail.nih.gov

Abbreviations used: BBB, blood–brain barrier; CNS, central nervous system; DTH, delayed-type hypersensitivity; EAE, experimental autoimmune encephalomyelitis; Eap, extracellular adherence protein; HUVEC, human umbilical vein endothelial cell; ICAM, intercellular adhesion molecule; MOG, myelin oligodendrocyte glycoprotein; MS, multiple sclerosis; PBT, peripheral blood T; VCAM, vascular cell adhesion molecule.

Multiple sclerosis (MS) and its animal model, experimental autoimmune encephalomyelitis (EAE), are demyelinating diseases of the central nervous system (CNS) mediated by autoreactive T cells that penetrate through the blood–brain barrier (BBB) into the brain parenchyma. These T cells initiate autoimmune responses against antigens in the myelin sheath of the CNS, including myelin basic protein or myelin oligodendrocyte protein (1). Thus, the recruitment of autoreactive lymphocytes represents a crucial pathogenetic event in initiating CNS inflammation, and interfering with the homing of these cells may represent a feasible therapeutic approach for both EAE and MS.

Lymphocyte extravasation requires a well-coordinated sequence of adhesive and signaling events, including selectin-mediated rolling, chemoattractant-induced integrin activation, integrin-dependent firm adhesion, and the subsequent transendothelial migration (2). During adhesion and transmigration, integrins of the β1 and β2 family, such as VLA-4 (α4β1) or LFA-1 (αLβ2), bind to their endothelial counter-receptors vascular cell adhesion molecule (VCAM)-1 and intercellular adhesion molecule (ICAM)-1, respectively. Numerous studies have shown that adhesion of lymphocytes to inflamed brain vessels during EAE is mainly mediated by the VLA-4–VCAM-1 system (3, 4), although there is also evidence pointing to the role of the LFA-1–ICAM-1 interaction (5; 6). Recent studies indicated that both systems may have a distinct contribution in the

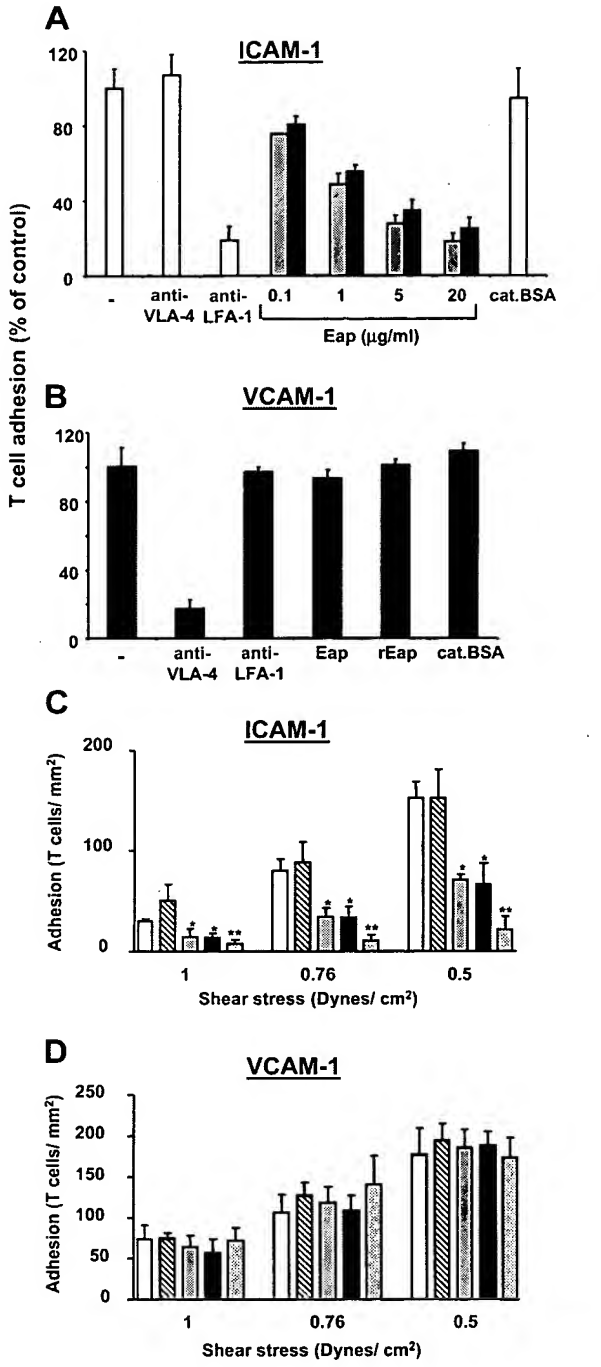

Figure 1. Eap inhibits T cell adhesion to ICAM-1. (A) The adhesion of T cells to immobilized ICAM-1 is shown in the absence (white bars) or presence of blocking mAb against VLA-4, mAb against LFA-1 (each at 20 μg/ml), increasing concentrations of purified (gray bars), or recombinant (black bars) Eap, or cationic BSA (20 μg/ml). (B) The adhesion of T cells to immobilized VCAM-1 is shown in the absence or presence of blocking mAb against VLA-4, mAb against LFA-1 (each at 20 μg/ml), purified Eap, recombinant Eap, or cationic BSA (each at 20 μg/ml). Cell adhesion is expressed relative to control (in the absence of competitor). Data are mean ± SD ($n = 3$) of a typical experiment; similar results were obtained in three separate experiments. (C and D) Adhesion of T cells to immobilized ICAM-1 (C) or VCAM-1 (D) under laminar shear flow conditions is shown in the absence (white bars) or presence of cationic BSA (diagonally striped bars), purified Eap (gray bars), recombinant Eap (black bars), or anti-LFA-1 mAb (dotted bars) (each at 20 μg/ml). Data are mean ± SEM, $n = 3$ separate experiments. *, $P < 0.05$. **, $P < 0.01$.

recruitment of encephalitogenic T cells. Although the VLA-4–VCAM-1 interaction predominantly mediates the initial adhesion to the inflamed vessels, LFA-1–ICAM-1 are engaged in the subsequent transendothelial migration of T cells (7, 8).

To date, therapeutic approaches targeting adhesion molecules have focused predominantly on the blockade of the VLA-4–VCAM-1 system (9). An antibody to VLA-4 that ameliorated EAE in mice was humanized (natalizumab) and demonstrated encouraging clinical efficacy for the treatment of patients with relapsing forms of multiple sclerosis. However, a few cases of fatal progressive multifocal leukoencephalopathy attributed to natalizumab prompted its withdrawal (9). Thus, the need for other adhesion molecule–based therapies is emerging. In contrast with the VLA-4–VCAM-1 system, only a few studies have addressed the role of the LFA-1–ICAM-1 system as a target in EAE, although ICAM-1 is clearly up-regulated in EAE and MS, and serum levels of soluble ICAM-1 were found to be elevated in MS patients with clinically symptomatic disease (5, 6, 10).

Extracellular adherence protein (Eap), also designated MHC class II analogous protein (Map) or P70, is a secreted protein from *Staphylococcus aureus*. Eap has a very broad repertoire of binding interactions to host extracellular matrix components (11, 12). Recently, we demonstrated a mechanism used by *S. aureus* to escape the host immune system that was attributed to the very potent antiinflammatory function of Eap. In particular, we found Eap to undergo a direct interaction with ICAM-1 that resulted in the disruption of integrin-dependent neutrophil–endothelial interactions (13). Strikingly, Eap was even more potent than blocking antibodies against the β2-integrin receptors or against ICAM-1.

These observations prompted us to investigate whether Eap could be feasible to interfere with T cell–adhesive mechanisms in EAE. In the present study, we show that Eap inhibits the LFA-1–ICAM-1 interaction and the T cell–endothelial interactions in vitro and in vivo. Furthermore, administration of Eap not only prevented the development of EAE, but Eap treatment reverted the disease and repressed its progress after its onset. Thus, Eap may represent a promising new therapy for chronic inflammatory diseases such as EAE and MS.

RESULTS

Eap blocks adhesion of T cells to ICAM-1

We have previously shown that Eap interferes with the interaction between ICAM-1 and its β2-integrin counterreceptors Mac-1 and LFA-1, thereby blocking neutrophil recruitment (13). To test whether Eap might interfere with T cell recruitment, we first examined the adhesion of peripheral blood T (PBT) cells to immobilized ICAM-1 and VCAM-1.

As shown in Fig. 1, the adhesion of PBT cells to immobilized ICAM-1 was mediated by LFA-1, whereas adhesion to VCAM-1 was dependent on β1-integrins. Under both static (Fig. 1, A and B) and physiologic flow conditions (Fig. 1, C and D), both purified and recombinant Eap dose-dependently inhibited the adhesion of PBT cells to immobilized ICAM-1, whereas adhesion of PBT cells to VCAM-1 was not affected in the presence of Eap. The inhibitory effect of Eap on the adhesion of PBT cells to ICAM-1 was comparable to the effect of blocking mAb to LFA-1 (Fig. 1). As Eap is a cationic protein, we engaged cationic BSA as a negative control, which did not affect LFA-1– or VLA-4–dependent adhesion to ICAM-1 or VCAM-1, respectively (Fig. 1).

Interference of Eap with T cell–endothelial cell interactions under static and physiologic flow conditions

As Eap blocks the adhesion of PBT cells to ICAM-1, we further determined whether Eap interferes with PBT cell–endothelial cell interactions. Therefore, the adhesion of PBT cells to endothelial cells as well as the transmigration of PBT cells through endothelial cell monolayers was studied under static and physiologic flow conditions. Under static conditions, the adhesion of PBT cells to TNF-α–prestimulated endothelial cells was mainly dependent on VLA-4, whereas the LFA-1–ICAM-1 system mediates a smaller portion of the T cell adhesion to endothelial cells under these conditions (Fig. 2 A). Both purified and recombinant Eap partially blocked adhesion of PBT cells to endothelial cells; the maximal inhibition observed was ~35–40% and was comparable to the inhibition obtained with blocking mAb to LFA-1 (Fig. 2 A). In contrast, transendothelial migration of PBT cells was predominantly mediated by the LFA-1–ICAM-1 interaction; in this case, both purified and recombinant Eap were more potent in blocking PBT cell transendothelial migration (Fig. 2 B). As a negative control, cationic BSA did not influence PBT cell adhesion or transmigration.

Because the PBT cell–endothelial cell interactions under physiologic flow conditions simulate in vivo physiological shear flow, we studied the effect of Eap under defined shear flow in vitro (14, 15). As previously reported, PBT cell adhesion to TNF-α–prestimulated endothelial cells under physiologic flow in vitro is mainly dependent on the VLA-4–VCAM-1 adhesion pathway and to a lesser extent on the LFA-1–ICAM-1 pathway, whereas transmigration was primarily LFA-1–ICAM-1 dependent (7, 14, 16). Consistent with these prior observations, here we show that purified or recombinant Eap (data with recombinant Eap not shown) as well as blocking mAb to LFA-1 had no statistically significant effect on adhesion of PBT cells to TNF-α–activated human umbilical vein endothelial cell (HUVEC) monolayers under flow conditions (Fig. 3 A), whereas transendothelial migration was significantly blocked by Eap or mAb to LFA-1 (Fig. 3 B). In contrast, no effect of cationic BSA was observed. Collectively, these data (Figs. 1–3) indicate that Eap interferes with the LFA-1–ICAM-1–dependent component of T cell–endothelial interaction pathway under both static and physiologic flow conditions in vitro. This inhibitory effect of Eap is specific and cannot be attributed to a nonspecific effect of the cationic charge of Eap.

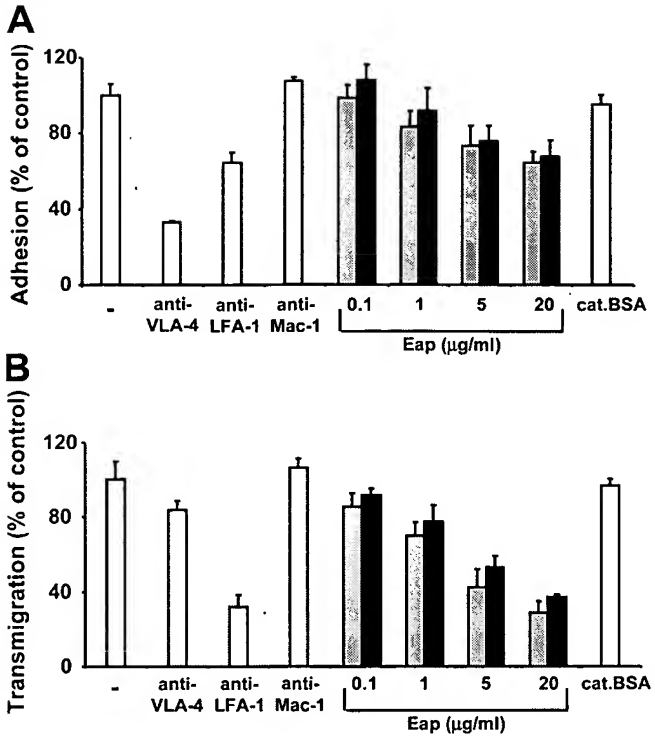

Figure 2. Eap inhibits T cell–endothelial cell interactions. (A) The adhesion of T cells to TNF-α prestimulated HUVEC (10 ng/ml, 16 h) is shown in the absence or presence of blocking mAb against VLA-4, blocking mAb against LFA-1, blocking mAb against Mac-1 (each at 20 μg/ml) (white bars), increasing concentrations of purified Eap (gray bars), recombinant Eap (black bars) or cationic BSA (20 μg/ml; white bars). (B) SDF-1α–stimulated transendothelial migration of T cells is shown in the absence (white bars) or presence of blocking mAb against VLA-4, blocking mAb against LFA-1, blocking mAb against Mac-1 (each at 20 μg/ml) (white bars), increasing concentrations of purified Eap (gray bars), recombinant Eap (black bars), or cationic BSA (20 μg/ml; white bars). Cell adhesion and cell transmigration is expressed relative to control (in the absence of competitor). Data are mean ± SD ($n = 3$) of a typical experiment; similar results were obtained in three separate experiments.

Inhibition of T cell recruitment and delayed type hypersensitivity (DTH) responses in vivo by Eap

To test whether Eap affects T cell–mediated immune responses in vivo, the ability of Eap to interfere with T cell recruitment and cellular immunity was assessed in a DTH model. DTH responses are mediated by infiltrating T cells in response to formerly encountered antigens, resulting in a specific inflammation at the site of local challenge. Mice immunized with oxazolone at day 0 and challenged locally on the right ear on day 5 developed a significant DTH response as measured by ear swelling at day 6 (Fig. 4). Mice treated systemically with either purified or recombinant Eap on day 5 (3 h before local challenge) had a significantly reduced DTH

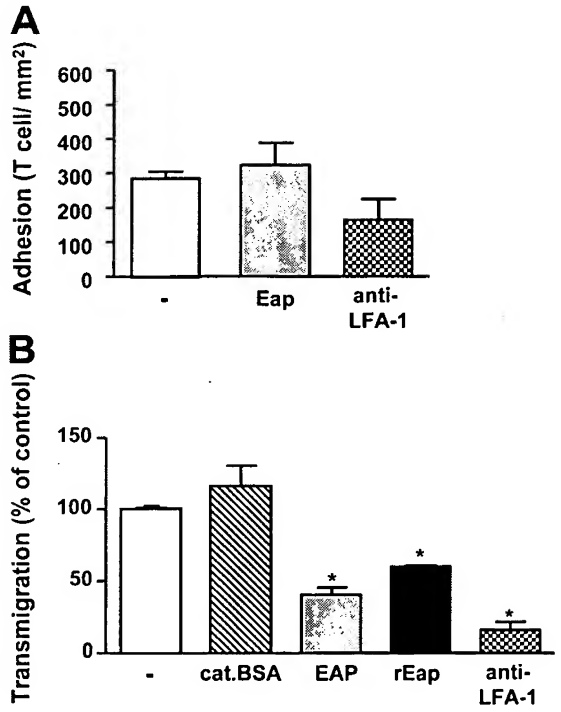

Figure 3. Effect of Eap on T cell–endothelial cell interactions under physiologic flow conditions. T cells were drawn across TNF-α–stimulated endothelial monolayers (25 ng/ml, 4 h) under laminar shear flow conditions (0.76 dynes/mm²). (A) The adhesion of T cells was studied without (white bar) or with purified Eap (gray bar) or anti-LFA-1 mAb (dotted bar) (each 20 μg/ml). (B) The transmigration of T cells was studied without (white bar) or with cationic BSA (diagonally striped bar), purified Eap (gray bar), recombinant Eap (black bar), or anti-LFA-1 mAb (dotted bar) (each 20 μg/ml). T cell adhesion (A) and transmigration relative to control (B) were determined as described in Materials and methods. Data are mean ± SEM, $n = 3$ separate experiments. *, $P < 0.05$.

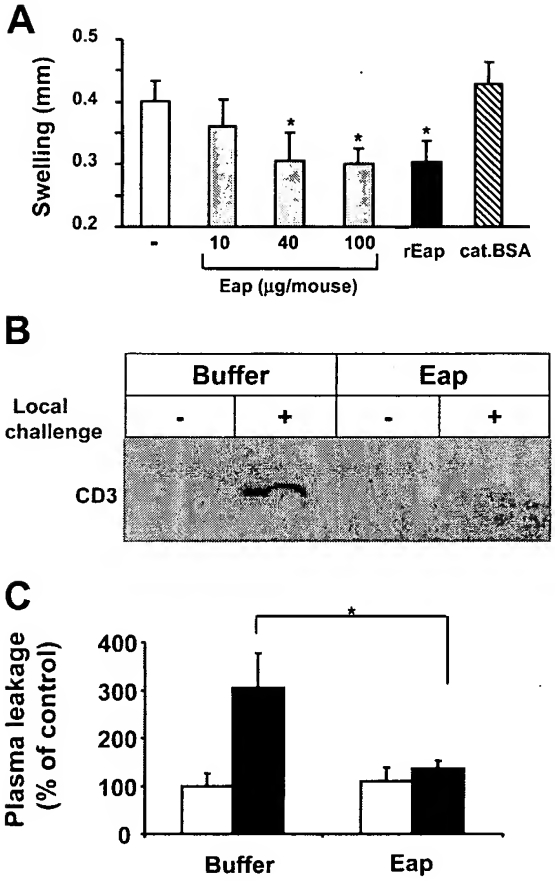

Figure 4. Inhibition of DTH response by Eap. (A) Mice were immunized with OXA (day 0) and at day 5 mice were challenged with local application of OXA on the ear. 2 h before local challenge, mice were treated without (white bar) or with increasing concentrations of purified Eap (gray bars), recombinant Eap (50 μg, black bar), or cationic BSA (100 μg, diagonally striped bar) administered intraperitoneally ($n = 5$ mice/group). Ear thickness was measured after 24 h. The difference in the ear thickness in mm is shown. Data are mean ± SD ($n = 7$). (B) The detection of infiltrated T cells is shown by detection of CD3 in Western blot. Ear tissues from DTH-induced mice that were treated with buffer or Eap were homogenized and the whole tissue lysates were subjected to Western blot to detect the amount of CD3. A typical Western blot for CD3 from the ears of buffer- or Eap-treated mice without (−) or with (+) local challenge using OXA is shown. (C) The vascular leakage (as assessed by influx of Evan's blue) of nonchallenged (white bars) or OXA challenged (black bars) ears is shown in mice pretreated with buffer ($n = 5$) or with Eap ($n = 5$). Ear tissue was removed, dried, and formamide was added to the dried ear tissue to extract Evan's blue; the optical density was registered at 590 nm, as a measure for the content of leaked Evan's blue. Plasma leakage is shown as percent of control (nonchallenged ear of buffer-treated mice) and data are mean ± SD ($n = 5$). *, $P < 0.03$.

response as compared with vehicle-treated but immunized control mice (Fig. 4 A). The effect of Eap was dose dependent and a significant decrease in ear thickness was observed with 40 and 100 μg of purified Eap/mouse ($P < 0.017$ and $P < 0.025$, respectively) (Fig. 4 A).

We examined whether Eap reduced DTH by blocking the local T cell infiltration into the challenged ear. Swollen ear tissues were extracted and homogenized, and equal amounts of tissue lysates were subjected to Western blot analysis for the detection of CD3. As shown in Fig. 4 B, Eap inhibited the recruitment of T cells as indicated by the significant decrease in detection of CD3 as compared with vehicle-treated mice. A major component of the DTH response leading to the ear swelling and the local edema is the increased vascular permeability that also promotes the increased transmigration and recruitment of lymphocytes. We therefore investigated whether Eap treatment reduced the plasma leakage into the inflamed ear by comparing the amounts of Evan's blue dye extracted from the ears of the mice treated with Eap or vehicle. The nonchallenged contralateral ears were used as control to determine the baseline of Evan's blue leakage. Eap treatment significantly reduced Evan's blue leakage by 50–60% compared with the vehicle-treated control (Fig. 4 C). Furthermore, Eap largely prevented TNF-α–induced increased permeability of an endothelial monolayer, as well as the TNF-α–induced morphological changes in the interendothelial junctions (unpublished data).

Prevention of EAE by Eap

Our data up to this point indicate that Eap inhibits T cell recruitment in vitro and in vivo. We therefore tested whether Eap could be used as a therapy in the EAE model. EAE is mediated by autoreactive T cells infiltrating the CNS. EAE was induced as described in Materials and methods and the average onset of the clinical symptoms defining the disease occurred on day 12 after immunization of C57BL/6 mice with myelin oligodendrocyte glycoprotein (MOG) peptides. To determine whether Eap prevents the development of EAE, we treated the immunized mice on days 11, 14, and 17 with purified or recombinant Eap. We tested 10, 25, and 50 μg concentrations of Eap administered on days 11, 14, and 17. Only a subtle reduction of EAE was achieved with 10 μg Eap; however, this reduction was not significant (difference in mean cumulative disease score, $P = 0.4$). In mice that received 25 μg of Eap, we observed an amelioration of EAE from day 18 (i.e., 1 d after completing the treatment on day 17), which remained obvious during the whole course of the experiment (difference in mean cumulative disease score, $P = 0.002$). More strikingly, mice that received 50 μg Eap only marginally developed EAE, with the mean clinical score not exceeding 1 at any time. The prevention of EAE development by 50 μg Eap was maintained throughout the study period (difference in mean cumulative disease score, $P < 0.001$) (Fig. 5 A). In addition, EAE was ameliorated by 50 μg of recombinant Eap (difference in mean cumulative disease score, $P < 0.001$) (Fig. 5 B). In contrast, cationic BSA did not affect the course of EAE, thus excluding a nonspecific effect of the cationic charge of Eap (Fig. 5 B).

However, in a clinical setting of MS, therapeutic intervention is started after the onset of the disease. Hence, the efficacy of Eap treatment for EAE was tested under such conditions. Strikingly, intervention with Eap after the onset of EAE on days 15, 17, and 19 (after initial immunization by MOG peptide) resulted in a prompt clinical recovery from EAE, which was significant even 2 d after the first Eap administration (day 17, $P < 0.032$). Interestingly, the recovery from EAE was sustained until the end of the study (day 33, $P < 0.008$) (Fig. 5 C). Overall, the mean cumulative disease score of Eap-treated mice was significantly lower than that of vehicle-treated mice ($P < 0.001$). In addition, consistent with our data and with the dramatic inhibitory effect on the clinical EAE symptoms by Eap, we found that mononuclear cell infiltrates were strongly reduced or almost absent in the brains of Eap-treated mice compared with the vehicle-treated mice that presented with perivascular and parenchymal inflammatory cell infiltrates (Fig. 6). Furthermore, the T cell recruitment to the brain was inhibited by Eap as indicated by the significant decrease in staining for CD3 in the brains of Eap-treated mice as compared with the brains of vehicle-treated mice (Fig. 6). Collectively, Eap prevented the development of EAE, as well as reverted the disease after its onset as a result of the propensity of the protein to block the infiltration of inflammatory T cells into the brain.

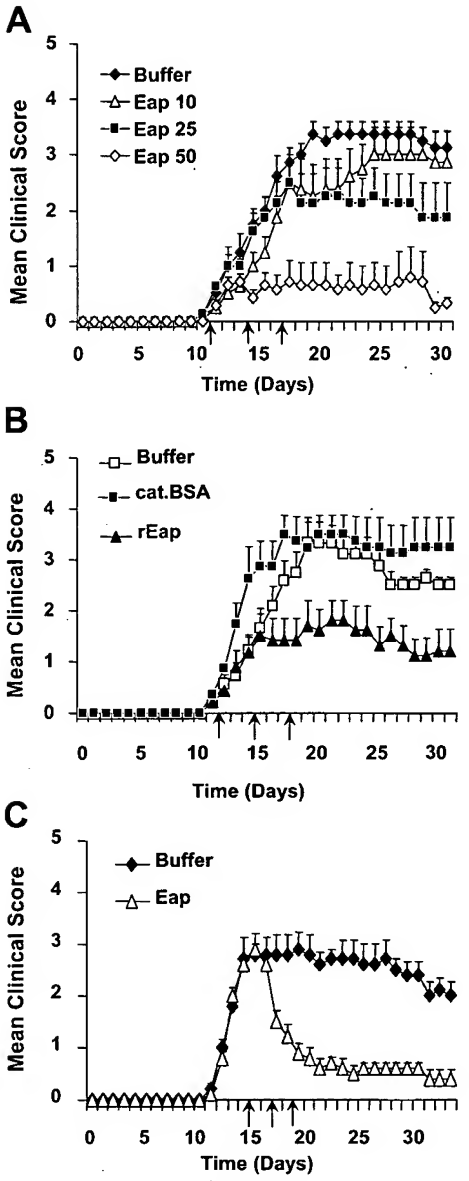

Figure 5. Inhibition of EAE by Eap. MOG-mediated EAE response in mice receiving different treatments. (A) Mice were treated with buffer (closed diamonds) or increasing concentrations of purified Eap (10 μg; open triangles; 25 μg; closed squares; 50 μg, open diamonds) that were administered on days 11, 14, and 17 (arrows) ($n = 5$–8 mice/group). (B) Mice were treated with buffer (open squares), recombinant Eap (50 μg, closed triangles), or cationic BSA (50 μg, closed squares) that were administered on days 11, 14, and 17 (arrows) ($n = 5$ mice/group). (C) Purified Eap (50 μg, open triangles) was administered on days 15, 17, and 19 (arrows) (i.e., after the onset of EAE; $n = 5$ mice/group). Data are represented as the mean clinical score and are mean ± SEM.

DISCUSSION

MS and its mouse counterpart, EAE, is a devastating disease with a very high mortality rate (17, 18). The inflammatory process associated with MS and EAE involves autoreactive T cells and additional cells of the immune system that infiltrate the CNS as well as the breakdown of the BBB (19). These

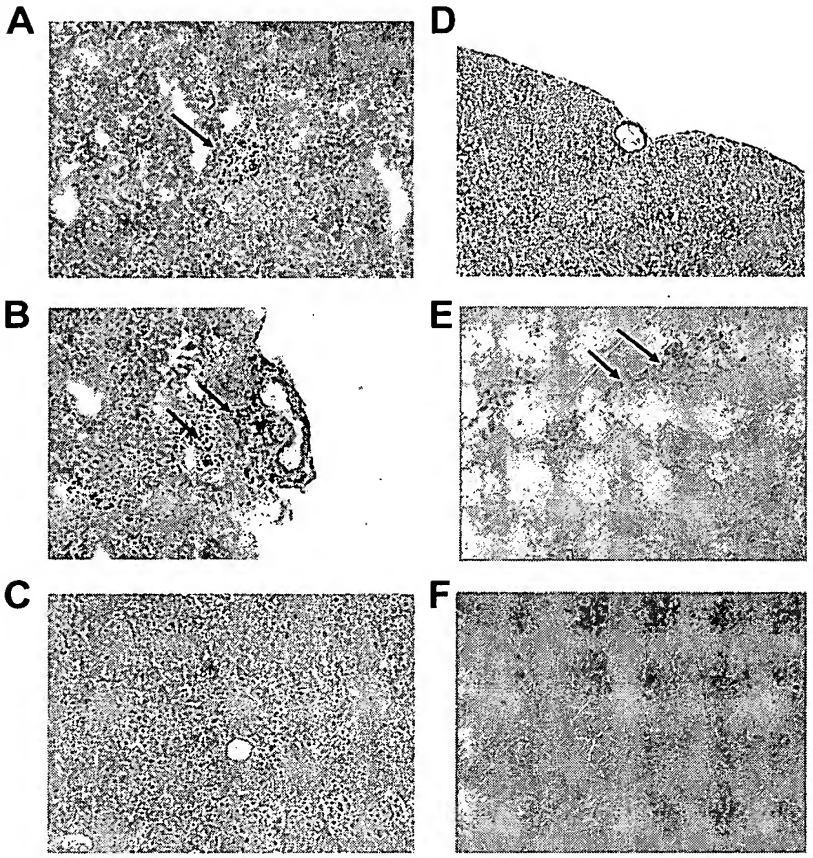

Figure 6. Eap inhibits the infiltration of the CNS by inflammatory cells during EAE. Histology (hematoxylin and eosin staining; A–D) and immunohistology (E–F) from brain sections of EAE mice. Typical photomicrographs indicating parenchymal (A) or perivascular (B) inflammatory cell infiltration in the CNS of buffer-treated mice during EAE. The arrows indicate the inflammatory cell infiltrates. No parenchymal or perivascular cell infiltration was noted in Eap-treated mice (C and D). Massive T cell infiltrates were noted in the brains of buffer-treated mice as indicated by the CD3 staining (E), whereas CD3-positive cells were hardly present in the brains of Eap-treated mice (F).

events are coordinated by chemokines and cytokines as well as by adhesion molecules expressed by both the immune cells and the activated endothelium, especially involving the VLA-4–VCAM-1 and the LFA-1–ICAM-1 adhesion systems (20). The need of therapies for MS and EAE particularly targeting adhesion molecules to limit T cell homing is growing, especially after the withdrawal of natalizumab, an antibody against VLA-4 that demonstrated encouraging efficacy in ameliorating clinical relapses of MS (9). The design of such therapies has to be specific in targeting to increase efficacy and reduce the risk of potential side effects. Our present work clearly demonstrates that the potent antiinflammatory *S. aureus*–derived Eap may provide the basis for the development of a promising novel therapeutic approach for the treatment of MS.

The following three features concur with a potent inhibitory effect of Eap on T cell recruitment in vitro and in vivo to effectively interfere with the development and progression of EAE. First, in vitro, purified and recombinant Eap specifically targeted LFA-1–ICAM-1– but not VLA-4–VCAM-1–mediated T cell recruitment. Consistent with a stronger involvement of the latter adhesion pathway in T cell adhesion to endothelial cells and of the former with T cell transendothelial migration (7, 8, 14, 16), we observed a strong inhibitory effect of Eap on T cell transendothelial migration as opposed to a weak inhibitory effect on T cell adhesion to endothelial cells under physiologic flow conditions. Second, in vivo, we found that purified and recombinant Eap blocked T cell recruitment and the consequent clinical responses to exogenous antigen in the DTH model. Our data in this model are consistent with a previous report by Lee et al. (21); although in that report, Eap was administered during both the induction and effector phases, whereas in our study administration of Eap during the effector phase was sufficient to block DTH. Moreover, we demonstrate here that Eap reduced the vascular permeability that occurred during the inflammatory response in DTH. Third, Eap prevented the development of EAE and markedly reduced infiltration of immune cells to the CNS. Strikingly, intervention with Eap after the onset of EAE clinical symptoms effectively suppressed EAE and reversed the clinical symptoms almost completely. Interestingly, the inhibitory effect of Eap on EAE persisted even after Eap was discontinued, whereas "rebound"

elevated EAE symptoms were observed after stopping administration of the antibody against VLA-4 (22). The inhibitory effects of Eap could not be attributed to its cationic charge because cationic BSA was not effective in any of the experimental systems used in our study.

Our finding that Eap blocks the LFA-1–ICAM-1 system as a therapeutic modality for EAE are in line with the delay of EAE onset by anti–LFA-1 or anti–ICAM-1 antibodies (5, 6). In contrast, ICAM-1–deficient mice exhibited enhanced EAE symptoms (23). A similar controversy has also been reported for PECAM-1–deficient mice, which were shown to have an earlier onset of EAE (24). Thus, besides differences in the animal strains and the experimental models used that may account for these discrepancies, it is clear that therapeutic studies may not correspond to studies with genetically manipulated mice.

Our data support the conclusion that Eap blocks EAE through interfering with the LFA-1–ICAM-1 adhesion pathway that mediates T cell recruitment most likely as a result of its inhibitory effect on transendothelial migration. Consistent with our findings, Laschinger et al. (8) demonstrated that encephalitogenic T cells use LFA-1 for transendothelial migration but not for adhesion to spinal cord microvessels in vivo. However, during the course of EAE, migration of immune cells to the CNS takes place in two phases (25). In the first phase, newly emigrated T lymphocytes recognize their antigen and trigger the inflammatory response, which leads to initiation of the second phase, during which the inflammation-dependent breakdown of the BBB and the intense secondary infiltration of other inflammatory cells such as macrophages is prominent (26). Activated T cells with a TH1 cytokine profile are central in coordinating these processes (27). This inflammatory response also involves the enhanced expression of adhesion molecules on the endothelial cells closely related to the damage of the BBB (28). As the LFA-1–ICAM-1 adhesion pathway mediates this secondary inflammatory cell recruitment in part, we speculate that Eap interferes with this process and thus accounts for the strong Eap-induced suppression of EAE, even after its onset. However, most studies to date have focused on the adhesive events regulating the infiltration of encephalitogenic T cells, although interfering with this secondary inflammatory response may be a more feasible therapeutic approach in a clinical setting where MS is diagnosed after its onset.

The LFA-1–ICAM-1 interaction is also involved in the antigen presentation process (29, 30, 31). However, our data demonstrate a therapeutic effect of Eap given during the effector phase of EAE and suppressing EAE after its onset. This indicates that, in our study, Eap cannot interfere with the induction phase to inhibit early interactions between immunocompetent cells after exposure to antigen. However, from a (patho-)biologic point of view, it would be intriguing to test whether Eap interferes with antigen presentation. The underlying mechanisms of the immunomodulatory role of Eap (13, 21) will be addressed in detail in future studies. Here, the recent crystallographic analysis of Eap revealed structural similarity to bacterial superantigens (32) that should also be taken into account as well.

The endothelium as an essential architectural component of the BBB plays a crucial role in CNS inflammation. Under physiological conditions, the BBB limits the infiltration of inflammatory cells to the CNS. However, the breakdown of the BBB is a hallmark in the development of EAE and MS, thereby potentiating the inflammatory response (33). Interestingly, we observed that Eap may reduce the TNF-α–induced disruption of endothelial cell contacts and the consequent increase in endothelial permeability in vitro (unpublished data) as well as the barrier dysfunction and plasma leakage in the DTH response in vivo. One could assume that Eap might also have a protective effect on the BBB during the course of EAE that may very well contribute to and account for its excellent therapeutic efficacy.

The advantages of the use of Eap as an antiadhesive treatment of EAE and MS may be manifold. One advantage is that Eap targets endothelial ICAM-1, which is up-regulated on the inflamed endothelium during the EAE (34, 35), whereas antibodies against VLA-4 target a constitutively expressed integrin on the lymphocytes as well as other types of leukocytes. Moreover, Eap seems to interfere specifically with LFA-1–ICAM-1–mediated transendothelial migration, which is downstream of the VLA-4–VCAM-1–mediated initial adhesion of encephalitogenic T cells. Another advantage is that Eap reversed EAE after its onset, whereas application of anti–VLA-4 prevented or ameliorated EAE only if it was initiated before the onset of disease and treatment with anti-VLA-4 during acute disease exacerbated EAE (36). A third advantage is that Eap may exert more beneficial effects as it may interfere with the inflammatory cell recruitment secondary to the infiltration of encephalitogenic T cells and may protect BBB breakdown. Together, our present work clearly demonstrates that Eap may prove a novel and promising therapy for the treatment of MS.

MATERIALS AND METHODS

Mice and cell culture. Female C57BL/6 mice were obtained from The Charles River Wiga and housed in the animal facilities of the University of Heidelberg. Mice were used between 10 and 12 wk of age. All animal studies were approved by the governmental office in Karlsruhe, Germany. HUVECs were cultivated in endothelial cell culture media from PromoCell as described previously (37). In experiments performed under flow conditions, HUVECs were isolated and cultured as described previously (15), and $CD3^+$ T cells were isolated from sodium-citrated anticoagulated whole blood drawn from healthy volunteers as described previously (15). Informed consent for blood donations was provided according to the Declaration of Helsinki and according to the Brigham and Women's Hospital Institutional Review Board–approved protocols for protection of human subjects.

Reagents. The following reagents were provided by the following sources: blocking mAb 6S6 against β1-chain (CD29) (Chemicon); blocking mAb LPM19c against Mac-1 (Acris); and mAb HP2.1 against integrin α4-chain, (Immunotech). Blocking mAb against LFA-1, L15 was provided by Y. van Kooyk (VU University Medical Center, Amsterdam, The Netherlands). Recombinant ICAM-1 and VCAM-1, TNF-α were obtained from R&D Systems. FITC-conjugated mAb to human CD3 for flow cytometry was obtained from BD Biosciences. Rat anti-mouse CD3 (MCA1477)

for Western blot and immunostaining as well as stromal cell–derived factor-1α (SDF1α) were obtained from Serotec. Cationic BSA was purchased from Sigma-Aldrich.

Eap purification. Eap from *S. aureus* strain Newman was purified as described previously with modifications (13). In brief, bacteria were harvested after a 20-h incubation in BHI medium (4 × 500 ml) at 37°C. The resultant 1-M lithium chloride-treated extract was dialyzed against PBS, concentrated, and adsorbed onto SP Sepharose (GE Healthcare) in loading buffer (30 mM phosphate buffer, pH 7.0, 200 mM NaCl) at 4°C overnight. After stepwise elution with increasing NaCl concentrations, the pooled eluted fractions (between 0.6 and 0.8 M NaCl) were dialyzed against 1:4 diluted PBS at 4°C and concentrated using Millipore centricon centrifugal filter devices (MWCO 30 kD; Millipore). The rententate (containing 2 mg/ml Eap) was further purified by cation exchange chromatography on Mono S 10/100 GL tricorn column using an ÄKTA fast performance liquid chromatography system (GE Healthcare), operated with 10 mM Tris/HCl, pH 8.0, and an increasing linear NaCl gradient (0–1 M NaCl). Eap-containing fractions were purified on a Superdex 75 HR 10/30 gel filtration column and equilibrated with TBS at pH 7.4, and Eap-positive fractions were pooled, concentrated by ultrafiltration (1–1.5 mg/ml), sterile filtered, and snap frozen at −80°C until further use. Eap revealed a single protein at 64 kD upon SDS-PAGE and was devoid of detectable endotoxin.

Expression and purification of recombinant Eap. A designer gene fragment encoding the entire predicted mature form of Eap from *S. aureus* strain Mu50 was PCR amplified from genomic DNA using oligonucleotides to append SalI and NotI sites at its 5′ and 3′ ends, respectively. The amplified product was digested with the appropriate restriction endonucleases, subcloned into the corresponding sites of the prokaryotic expression vector pT7HMT (38), and sequenced in its entirety to confirm the integrity of the Eap coding region.

After sequencing, the Eap expression plasmid was transformed into *Escherichia coli* strain BL21 (DE3) and the resulting strain was cultured, induced, harvested, and lysed under denaturing conditions according to published protocols (38). After centrifugation (25,000 *g* for 30 min at 20°C), the clarified extract from 1 L of original culture was applied to a 7.5-ml column of chelating sepharose fast flow (GE Healthcare) that had been previously charged with Ni_2SO_4 and equilibrated at 20°C in denaturing wash buffer (20 mM NaH_2PO_4, pH 6.0, 500 mM NaCl, 20 mM imidazole, 8 M urea). Once the entire sample had entered the column, contaminating proteins were washed away with 75 ml of denaturing wash buffer and the specifically bound proteins were eluted with 15 ml of a similar buffer containing 200 mM imidazole. The denatured, purified Eap was refolded by rapid dilution into 150 ml of native binding buffer as described previously (20 mM Tris, pH 8.0, 0.5 M NaCl; reference 38). Then, the refolded recombinant Eap was concentrated by application to an identical chelating column equilibrated at 4°C in native binding buffer. Once the entire sample had entered, the column was washed with 75 ml of native binding buffer and the bound proteins were eluted with 15 ml of a similar buffer containing 500 mM imidazole.

After initial purification, the vector-encoded affinity tag was proteolytically removed from Eap by digestion with recombinant Tobacco Etch Virus protease as described previously (38). Once digestion was complete (as judged by SDS-PAGE), the entire proteolysis reaction was buffer exchanged into 20 mM ethanolamine, pH 9.0, using a HiPrep 26/10 Desalting column (GE Healthcare). Untagged Eap was separated from the residual protease and affinity tagged by cation-exchange chromatography on a 6-ml Resource S column (GE Healthcare), where the bound proteins were resolved by gradient elution to 1 M NaCl in ethanolamine buffer over 60 ml. The final purity of Eap was estimated at >95% (as judged by SDS-PAGE) with a yield of ~15 mg Eap per liter of original culture. Purified Eap was buffer exchanged into double-deionized water, lyophilized, and stored at −80°C before reconstitution. The final Eap protein contained the additional residues Gly-Ser-Thr at its amino terminus as a result of the subcloning and proteolysis procedures.

Preparation of PBT cells. Human PBMCs were isolated from heparin anticoagulated blood from healthy donors by Histopaque-1107 (Sigma-Aldrich) density gradient centrifugation. PBT cells were separated and purified from PBMCs using Pan-T cells isolation kit obtained from Miltenyi Biotec. The purity of T cells was shown to be >97% measured as CD3 positive using flow cytometry.

PBT adhesion to endothelial cells and transendothelial migration under static conditions. Adhesion of PBT cells to immobilized ICAM-1 or VCAM-1 or to cultured monolayers of HUVECs prestimulated for 16 h with TNF-α was tested as described previously (37, 39). In brief, plates were coated with ICAM-1 or VCAM-1 (10 μg/ml each) in PBS for 16 h at 4°C. HUVECs were grown to confluency onto 96-well plates and were stimulated for 16 h with TNF-α, and medium was changed before the addition of PBT cells. Fluorescently labeled PBT cells (10^5/well) were washed twice and added to the ICAM-1– or VCAM-1–coated wells or to HUVECs and were incubated at 37°C for 60 min in the absence or presence of inhibitors. After washing, adhesion of PBT cells was quantified using a fluorescence microplate reader (Bio-Tek).

Transendothelial migration was performed as described previously (39). In brief, transmigration assays were performed using 6.5-mm transwell filters with a 5-μm pore size (Corning Costar). After inserts were coated with gelatine (Sigma-Aldrich), HUVECs were seeded onto transwell filters 2 d before the assay and grown without medium in the lower compartment for 48 h in a humidified atmosphere (37°C, 5% CO_2). At the beginning of the transmigration assay, 600 μl migration assay medium (serum-free RPMI 1640 in the absence or presence of SDF1α) was added to the lower compartment of the transwell system. PBT cells (3×10^5 in 100 μl) were added to the upper compartment on top of the endothelial monolayer. After incubation for 4 h at 37°C the number of transmigrated cells in the lower compartment was estimated with a cell-counter (CASY-Counter; Schärfe-System). The inserts were washed twice in PBS and fixed with methanol, stained with crystal violet, and mounted on glass slides to confirm the confluence of the endothelial monolayer of the filters after the assay.

PBT adhesion and transmigration assays under physiological flow conditions. Glass coverslips (25-mm dia, Carolina Biological Supply) were coated with 2.5 μg/ml of ICAM-1 or VCAM-1 and 2 μg/ml of stromal cell-derived factor-1α (CXCL12, SDF-1α)(Peprotech). SDF-1α pretreatment has been shown to promote T cell adhesion to the integrin ligands (14). Where indicated, coverslips were treated with purified Eap, recombinant Eap, or cationic BSA or T cells were treated with function-blocking anti–LFA-1 mAb (TS1/22; American Type Culture Collection). PBT cell interactions with immobilized ICAM-1 or VCAM-1 were examined under conditions of fluid shear stress in a parallel plate flow chamber as described previously (40). In brief, PBT cells were drawn through the chamber at decreasing flow rates corresponding to an estimated shear stress of 1 dyne/cm², 0.76 dynes/cm², and 0.5 dynes/cm². T cell accumulation was determined after the initial minute of each flow rate by counting the number of cells in four different fields. T cell interactions with substrates were recorded using a 20× phase contrast objective, videomicroscopy, and VideoLab software. For PBT cell adhesion to HUVECs and transendothelial migration, confluent HUVECs grown on 25-mm dia glass coverslips coated with 5 μg/ml fibronectin (Sigma-Aldrich) were stimulated with TNF-α (25 ng/ml) for 4 h and inserted into the flow chamber. Where indicated, HUVECs were treated with 20 μg/ml Eap. Lymphocytes (10^6/ml) suspended in flow buffer (Dulbecco phosphate-buffered saline/0.1% human serum albumin) were drawn across HUVECs at 0.76 dyne/cm² for 3 min, followed by buffer alone for 10 min. HUVEC monolayers were incubated with 50 ng/ml of SDF-1α during 15 min before assay to promote T-lymphocyte TEM (14, 41). Live-cell imaging of leukocyte TEM was performed using a digital imaging system coupled to a Nikon TE2000 inverted microscope as described previously (15). Sequential images of differential interference contrast (DIC) were taken every 15 s for 10 min in a representative field from 3 min after the start of leukocyte perfusion. The total number of accumulated leukocytes

was determined by counting total adherent and transmigrated cells in five fields. The percentage of TEM = total transmigrated leukocytes/(total adhered + transmigrated leukocytes) × 100. $P \leq 0.05$ was considered statistically significant using the paired Student's *t* test or one-way analysis of variance for multiple groups.

DTH responses. Mice were sensitized by topical application of a 2% oxazolone (4-ethoxymethylene-2-phenyl-2-oxazoline-5-one; OXA; Sigma-Aldrich) solution in acetone/olive oil (4:1 vol/vol) onto the shaved abdomen (50 µl) (day 0). On day 5, the right ears were challenged by topical application of 10 µl of a 1% oxazolone solution on both sides of the ear, whereas the left ears were treated with vehicle alone. 3 h before local challenge, mice were treated with different concentrations of purified or recombinant Eap administered intraperitoneally. Ear thickness was measured after 24 h (day 6) using a spring-loaded micrometer (Mitutoyo). Measurement of ear thickness was performed by a researcher who was not aware of the treatment groups. The ear swelling was calculated by the difference in the thickness between right ears (OXA treated) and left ears (vehicle treated).

For the detection and quantification of CD3, ear tissues from DTH-induced mice were homogenized and equal amounts of tissue lysates were subjected to SDS-PAGE. Western blot analysis with antibody MCA1477 was performed to detect CD3.

Measurement of vascular leakage. Vascular leakage was measured as described previously (42). DTH-induced mice were injected intracardially with 100 µl Evan's blue dye (30 mg/kg) 24 h after OXA challenge. After 10 min, mice were killed and ear tissues were removed, dried at 55°C overnight, and weighed. Evan's blue was extracted from the dried ear tissue by incubation in formamide for 48 h and absorbance was measured at 590 nm in a microplate reader (BIO-TEK).

Induction of EAE. MOG p35–55, MEVGWYRSPFSRVVHLYRNGK, was purchased from TebuBio. Mice were immunized with 200 µg MOG peptide emulsified in Freund's incomplete adjuvant (Sigma-Aldrich) together with 5 mg/ml *Mycobacterium tuberculosis* H37RA (Difco). A total of 100 µl emulsion was subcutaneously injected into four sites on the flanks of mice near the tail. At days 0 and 2 after the initial peptide injections, animals received additional injections of 400 ng pertussis toxin (Difco) intraperitoneally. Different concentrations of purified or recombinant Eap or cationic BSA in 400 µl PBS (or the same volume of vehicle) were administered intraperitoneally at the times indicated in the figure legends.

Mice were scored daily for clinical assessment of disease based on the following criteria: 0, normal; 1, limp tail or hind limb weakness; 2, limp tail and hind limb weakness; 3, partial hind limb paralysis; 4, complete hind limb paralysis; and 5, moribund or dead. Food and water was made accessible to immobile animals, and moribund animals with a score of 5 were killed. A score of 5 was not included in the calculation of daily mean clinical score. Clinical scoring was performed by a researcher who was not aware of the treatment groups.

For the histological and immunohistological analysis of the CNS in the EAE model, mice brains were snap frozen in liquid nitrogen and embedded in OCT compound. Specimens were cut into 3-µm cross sections. To evaluate CNS infiltrates, sections were stained with hematoxylin and eosin or anti-CD3 mAb followed by eosin counterstaining.

Statistical analysis. For the analysis of the effect of Eap on the DTH response, one-way analysis of variance with Holm-Sidak post-hoc analysis (α value was set to 0.05) was performed. For the analysis of the effect of Eap on EAE, the Mann-Whitney U test was used for comparison between groups. Statistical analysis was performed by using SigmaStat3.1 (Systat Software Inc.).

We acknowledge U. Schubert and A. Sobke for technical assistance and Dr. G.M. Shearer for critically reading this manuscript.

This work was supported in part by the Intramural Research Program of the National Institutes of Health (NIH), National Cancer Institute (to T. Chavakis); by grants from the Deutsche Forschungsgemeinschaft: nos. SFB405 (to T. Chavakis) and SPP1130 (to T. Chavakis, M. Herrmann, K.T. Preissner); by NIH grant nos. HL56985, HL36028, and HL53393 (to F.W. Luscinskas); by a Fullbright/Spanish Ministry of Education and Science grant (to P. Alcaide), and by grant no. 2509 from the University of Missouri Research Board (to B.V. Geisbrecht).

The authors have no conflicting financial interests.

Submitted: 19 August 2005
Accepted: 10 March 2006

REFERENCES

1. 't Hart, B.A., and S. Amor. 2003. The use of animal models to investigate the pathogenesis of neuroinflammatory disorders of the central nervous system. *Curr. Opin. Neurol.* 16:375–383.
2. Springer, T.A. 1994. Traffic signals for lymphocyte recirculation and leukocyte emigration: the multistep paradigm. *Cell.* 76:301–314.
3. Yednock, T.A., C. Cannon, L.C. Fritz, F. Sanchez-Madrid, L. Steinman, and N. Karin. 1992. Prevention of experimental autoimmune encephalomyelitis by antibodies against $\alpha4\ \beta1$ integrin. *Nature.* 356:63–66.
4. Baron, J.L., J.A. Madri, N.H. Ruddle, G. Hashim, and C.A. Janeway Jr. 1993. Surface expression of $\alpha4$ integrin by CD4 T cells is required for their entry into brain parenchyma. *J. Exp. Med.* 177:57–68.
5. Gordon, E.J., K.J. Myers, J.P. Dougherty, H. Rosen, and Y. Ron. 1995. Both anti-CD11a (LFA-1) and anti-CD11b (MAC-1) therapy delay the onset and diminish the severity of experimental autoimmune encephalomyelitis. *J. Neuroimmunol.* 62:153–160.
6. Archelos, J.J., S. Jung, M. Maurer, M. Schmied, H. Lassmann, T. Tamatani, M. Miyasaka, K.V. Toyka, and H.P. Hartung. 1993. Inhibition of experimental autoimmune encephalomyelitis by an antibody to the intercellular adhesion molecule ICAM- 1. *Ann. Neurol.* 34:145–154.
7. Oppenheimer-Marks, N., L.S. Davis, D.T. Bogue, J. Ramberg, and P.E. Lipsky. 1991. Differential utilization of ICAM-1 and VCAM-1 during the adhesion and transendothelial migration of human T lymphocytes. *J. Immunol.* 147:2913–2921.
8. Laschinger, M., P. Vajkoczy, and B. Engelhardt. 2002. Encephalitogenic T cells use LFA-1 for transendothelial migration but not during capture and initial adhesion strengthening in healthy spinal cord microvessels in vivo. *Eur. J. Immunol.* 32:3598–3606.
9. Steinman, L. 2005. Blocking adhesion molecules as therapy for multiple sclerosis: natalizumab. *Nat. Rev. Drug Discov.* 4:510–518.
10. Cannella, B., A.H. Cross, and C.S. Raine. 1993. Anti-adhesion molecule therapy in experimental autoimmune encephalomyelitis. *J. Neuroimmunol.* 46:43–55.
11. Harraghy, N., M. Hussain, A. Haggar, T. Chavakis, B. Sinha, M. Herrmann, and J.I. Flock. 2003. The adhesive and immunomodulating properties of the multifunctional *Staphylococcus aureus* protein Eap. *Microbiology.* 149:2701–2707.
12. Chavakis, T., K. Wiechmann, K.T. Preissner, and M. Herrmann. 2005. *Staphylococcus aureus* interactions with the endothelium: the role of bacterial "secretable expanded repertoire adhesive molecules" (SERAM) in disturbing host defense systems. *Thromb. Haemost.* 94:278–285.
13. Chavakis, T., M. Hussain, S.M. Kanse, G. Peters, R.G. Bretzel, J.I. Flock, M. Herrmann, and K.T. Preissner. 2002. *Staphylococcus aureus* extracellular adherence protein serves as anti-inflammatory factor by inhibiting the recruitment of host leukocytes. *Nat. Med.* 8:687–693.
14. Cinamon, G., V. Shinder, and R. Alon. 2001. Shear forces promote lymphocyte migration across vascular endothelium bearing apical chemokines. *Nat. Immunol.* 2:515–522.
15. Rao, R.M., T.V. Betz, D.J. Lamont, M.B. Kim, S.K. Shaw, R.M. Froio, F. Baleux, F. Arenzana-Seisdedos, R. Alon, and F.W. Luscinskas. 2004. Elastase release by transmigrating neutrophils deactivates endothelial-bound SDF-1α and attenuates subsequent T lymphocyte transendothelial migration. *J. Exp. Med.* 200:713–724.
16. Luscinskas, F.W., H. Ding, and A.H. Lichtman. 1995. P-selectin and vascular cell adhesion molecule 1 mediate rolling and arrest, respectively, of $CD4^+$ T lymphocytes on tumor necrosis factor α-activated vascular endothelium under flow. *J. Exp. Med.* 181:1179–1186.

17. Lublin, F.D. 2005. Clinical features and diagnosis of multiple sclerosis. *Neurol. Clin.* 23:1–15 (v.).
18. Flachenecker, P., and P. Rieckmann. 2004. Health outcomes in multiple sclerosis. *Curr. Opin. Neurol.* 17:257–261.
19. Sospedra, M., and R. Martin. 2005. Immunology of multiple sclerosis. *Annu. Rev. Immunol.* 23:683–747.
20. Kennedy, K.J., and W.J. Karpus. 1999. Role of chemokines in the regulation of Th1/Th2 and autoimmune encephalomyelitis. *J. Clin. Immunol.* 19:273–279.
21. Lee, L.Y., Y.J. Miyamoto, B.W. McIntyre, M. Hook, K.W. McCrea, D. McDevitt, and E.L. Brown. 2002. The *Staphylococcus aureus* Map protein is an immunomodulator that interferes with T cell-mediated responses. *J. Clin. Invest.* 110:1461–1471.
22. Brocke, S., C. Piercy, L. Steinman, I.L. Weissman, and T. Veromaa. 1999. Antibodies to CD44 and integrin α4, but not L-selectin, prevent central nervous system inflammation and experimental encephalomyelitis by blocking secondary leukocyte recruitment. *Proc. Natl. Acad. Sci. USA.* 96:6896–6901.
23. Samoilova, E.B., J.L. Horton, and Y. Chen. 1998. Experimental autoimmune encephalomyelitis in intercellular adhesion molecule-1-deficient mice. *Cell. Immunol.* 190:83–89.
24. Graesser, D., A. Solowiej, M. Bruckner, E. Osterweil, A. Juedes, S. Davis, N.H. Ruddle, B. Engelhardt, and J.A. Madri. 2002. Altered vascular permeability and early onset of experimental autoimmune encephalomyelitis in PECAM-1-deficient mice. *J. Clin. Invest.* 109:383–392.
25. Chavarria, A., and J. Alcocer-Varela. 2004. Is damage in central nervous system due to inflammation? *Autoimmun. Rev.* 3:251–260.
26. Hickey, W.F. 1999. Leukocyte traffic in the central nervous system: the participants and their roles. *Semin. Immunol.* 11:125–137.
27. Krakowski, M.L., and T. Owens. 1997. The central nervous system environment controls effector $CD4^+$ T cell cytokine profile in experimental allergic encephalomyelitis. *Eur. J. Immunol.* 27:2840–2847.
28. Karpus, W.J., and R.M. Ransohoff. 1998. Chemokine regulation of experimental autoimmune encephalomyelitis: temporal and spatial expression patterns govern disease pathogenesis. *J. Immunol.* 161:2667–2671.
29. Jenkins, M.K., and J.G. Johnson. 1993. Molecules involved in T-cell costimulation. *Curr. Opin. Immunol.* 5:361–367.
30. Sharpe, A.H. 1995. Analysis of lymphocyte costimulation in vivo using transgenic and 'knockout' mice. *Curr. Opin. Immunol.* 7:389–395.
31. Lebedeva, T., M.L. Dustin, and Y. Sykulev. 2005. ICAM-1 co-stimulates target cells to facilitate antigen presentation. *Curr. Opin. Immunol.* 17:251–258.
32. Geisbrecht, B.V., B.Y. Hamaoka, B. Perman, A. Zemla, and D.J. Leahy. 2005. The crystal structures of EAP domains from *Staphylococcus aureus* reveal an unexpected homology to bacterial superantigens. *J. Biol. Chem.* 280:17243–17250.
33. Petty, M.A., and E.H. Lo. 2002. Junctional complexes of the blood-brain barrier: permeability changes in neuroinflammation. *Prog. Neurobiol.* 68:311–323.
34. Sharief, M.K., M.A. Noori, M. Ciardi, A. Cirelli, and E.J. Thompson. 1993. Increased levels of circulating ICAM-1 in serum and cerebrospinal fluid of patients with active multiple sclerosis. Correlation with TNF-α and blood-brain barrier damage. *J. Neuroimmunol.* 43:15–21.
35. Lou, J., M. Chofflon, C. Juillard, Y. Donati, N. Mili, C.A. Siegrist, and G.E. Grau. 1997. Brain microvascular endothelial cells and leukocytes derived from patients with multiple sclerosis exhibit increased adhesion capacity. *Neuroreport.* 8:629–633.
36. Theien, B.E., C.L. Vanderlugt, T.N. Eagar, C. Nickerson-Nutter, R. Nazareno, V.K. Kuchroo, and S.D. Miller. 2001. Discordant effects of anti-VLA-4 treatment before and after onset of relapsing experimental autoimmune encephalomyelitis. *J. Clin. Invest.* 107:995–1006.
37. Chavakis, T., A. Bierhaus, N. Al-Fakhri, D. Schneider, S. Witte, T. Linn, M. Nagashima, J. Morser, B. Arnold, K.T. Preissner, and P.P. Nawroth. 2003. The pattern recognition receptor (RAGE) is a counterreceptor for leukocyte integrins: a novel pathway for inflammatory cell recruitment. *J. Exp. Med.* 198:1507–1515.
38. Geisbrecht, B.V., S. Bouyain, and M. Pop. 2006. An optimized system for expression and purification of secreted bacterial proteins. *Protein. Expr. Purif.* 46:23–32.
39. Chavakis, T., T. Keiper, R. Matz-Westphal, K. Hersemeyer, U.J. Sachs, P.P. Nawroth, K.T. Preissner, and S. Santoso. 2004. The junctional adhesion molecule-C promotes neutrophil transendothelial migration in vitro and in vivo. *J. Biol. Chem.* 279:55602–55608.
40. Lim, Y.C., L. Henault, A.J. Wagers, G.S. Kansas, F.W. Luscinskas, and A.H. Lichtman. 1999. Expression of functional selectin ligands on Th cells is differentially regulated by IL-12 and IL-4. *J. Immunol.* 162: 3193–3201.
41. Muller, W.A. 2001. Migration of leukocytes across endothelial junctions: some concepts and controversies. *Microcirculation.* 8:181–193.
42. Kunstfeld, R., S. Hirakawa, Y.K. Hong, V. Schacht, B. Lange-Asschenfeldt, P. Velasco, C. Lin, E. Fiebiger, X. Wei, Y. Wu, et al. 2004. Induction of cutaneous delayed-type hypersensitivity reactions in VEGF-A transgenic mice results in chronic skin inflammation associated with persistent lymphatic hyperplasia. *Blood.* 104:1048–1057.

APPENDIX 3

Mouse Models

We have chosen mouse models for three devastating and common human neurological diseases—multiple sclerosis, Alzheimer's disease, and Parkinson's disease. These models provide a well-delimited workspace for our collaboration and maintain firm linkage to the two active Human BIRN test-beds and the BIRN-CC. All three diseases have mixed genetic and environmental etiologies and are sufficiently complex to be challenging from a bioinformatics perspective.

Parkinson's Disease, the Alpha Synuclein Mouse Model

The project efforts are focused on the development and application of correlated imaging approaches (confocal and electron microscopy, in vivo microscopic MRI) to Parkinson's disease (PD)—applied first to recently generated transgenic animal models of PD. Knowledge gained from this project will facilitate the assessment of neuropathologies and effectiveness of possible chemotherapeutic treatments for PD.

The overall goals for this project are to:

1. Characterize the phenotypic differences between transgenic alpha synuclein and wildtype mice at three levels:

- Gross level
- Regional/cellular level
- High resolution distribution maps of molecular constituents

2. Integrate multi-scale data into the BIRN

3. Establish collaborations with other groups and bring additional PD models for comparison

Multiple Sclerosis, the EAE Mouse Model

The pathology of Experimental Autoimmune Encephalomyelitis (EAE) is characterized by lymphocytic and mononuclear cell infiltration of the CNS, an increase in blood-brain barrier permeability, astrocytic hypertrophy, and often demyelination, all of which contribute to the observed clinical expression of disease, imbalance, and paralysis. This particular mouse model of EAE exhibits lesions in the C57BL/6 mouse in the brain within 45 days of the antigenic challenge. Because the clinical and pathological aspects of this disease bear significant similarities to multiple sclerosis (MS) it is a valuable model of that human demyelinating disease.

The brains of these mice are visualized using Magnetic Resonance Microscopy (MRM), histology, and immunohistochemistry. Lesions in these brains have been identified using these methods. The data are reconstructed into 3D volumes and registered into a common and defined coordinate system and atlased. This atlased information serves as a valuable tool for the collection and comparison of data in this model of MS as well as for future investigation of potential treatments.

Alzheimer's Disease, Tet-off APP Transgenic Mouse Model

Alzheimer's disease is thought to arise from the accumulation of a small peptide termed amyloid- b that is normally found in healthy individuals, but is abnormally abundant in the brains of AD patients. The Ab peptide aggregates into extracellular lesions or amyloid plaques that are found throughout the hippocampus and cortex of affected individuals. Both amyloid pathology and the cognitive decline associated with AD can be recreated in transgenic mouse models for the disease. Mice overexpressing the human amyloid precursor protein (APP) with mutations identified from families with inherited AD generate high levels of Ab and form amyloid plaques similar to those used found in the brains of patients with AD.

The mouse BIRN will examine a transgenic mouse model for AD in which the expression of APP can be controlled with antibiotic treatment. We anticipate that this controllable transgenic mouse model can be used with MRI and the other methods employed by collaborators in the mouse BIRN to study the long-term kinetics of amyloid lesions in the brain under conditions similar to those expected from future AD therapies.

In This Sec

Mouse BIRN Overview

Mouse BIRN (mBIRN) is a research and development effort funded by the National Center for Research Resources (NCRR) to produce an integrated framework for the collection, analysis, management, and visualization of diverse neuroscience data sets. It provides a test bed for the formulation of hardware, software, and protocols to produce a distributed adaptive database and multiscale, multimodality digital atlases of the mouse brain. These resrouces are used to share and mine multi-scale structural and functional data and integrate these with genomic and gene expression data. The goal is to create an infrastructure that can greatly enhance previously disparate data collections into a single system capable of quantitative visualization and linkage with previously disconnected knowledge bases.

Significance

mBIRN is acquiring complete volumetric coverage with MR, cryosections, conventional histology, and gene expression from the same specimen along with confocal light microscopy, and electron tomography from closely related specimens. This allows the neuroscientists studying the mouse models the ability to view the complex anatomy of the mouse brain in 3 dimensions at multiple scales for tissue and structure differentiation, along any arbitrary plane, and all from a single computer screen.

Combing these techniques with well characterized mouse models, gives us a powerful tool for investigating the disease mechanism and potential therapies. The development of MR microscopy in mouse models makes transition of imaging studies possible from mouse to human. mBIRN will complete the link making correlation possible between fundamental structural units (e.g., the dendritic spine), gene expression, traditional histology, magnetic resonance histology, and in vivo MR imaging. The products of mBIRN, including the initial data sets for these models, the tools for comparison, the infrastructure for sharing the data and the knowledge base, will all clearly be extensible to a much broader community as scientists seek to connect an exponentially increasing number of mouse models to human disease.

View the Mouse BIRN overview pdf.

Participants

mBIRN integrates the activities of five existing laboratories:

- The MRI Center in the Biological Imaging Center (BIC) at the California Institute of Technology (CIT)
- The Center for In Vivo Microscopy (CIVM) at Duke University
- The Laboratory of Neuro Imaging (LONI) at the University of California at Los Angeles (UCLA)
- The National Center for Microscopy and Imaging Research (NCMIR) at the University of California at San Diego (UCSD)
- The Informatics Center for Mouse Neurogenetics at UTHSC, Drexel, and BIDMC (Mouse Brain Library and The GeneNetwork)

These laboratories are connected by the networking and software infrastructure that is being co-developed with the BIRN Central Coordinating site (BIRN-CC).

Research

We have chosen mouse models for three devastating and common human neurological diseases-multiple sclerosis, Alzheimer's disease, and Parkinson's disease. These models provide a well-delimited workspace for our collaboration and maintain firm linkage to the two active Human BIRN test-beds and the BIRN-CC. All three diseases have mixed genetic and environmental etiologies and are sufficiently complex to be challenging from a bioinformatics perspective.

These models came into the mouse BIRN project as part of collaborative mechanisms and act to drive development of an open data sharing infrastructure. Our collaborators include:

Dr. Joanna Jankowsky at Caltech for the Alzheimer's disease model (APP)

Dr. Rhonda Voskuhl at UCLA for the multiple sclerosis model (EAE)
http://www.neurology.ucla.edu/faculty/VoskuhlR.htm

Dr. Eliezer Masliah at UCSD for the Parkinson's disease model (alpha synuclein-SNCA)
http://medicine.ucsd.edu/neurosci/the-faculty/masliah.html

These individuals are leaders in the field of neurodegenerative diseases, and all have substantial practical experience managing, exploiting, and interpreting results generated using these three models.

In This Se

- Mouse E
- Projects
- Resourc
- Mouse E Commu
- News ar

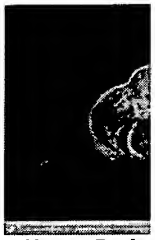

Mouse Brain Anim